Journal of Asian Earth Sciences 141 (2017) 59–73

Contents lists available at ScienceDirect

Journal of Asian Earth Sciences

journal homepage: www.elsevier.com/locate/jseaes

Full length Article

Early paleozoic granodioritic plutons in the Shedong W–Mo ore district, Guangxi, southern China: Products of re-melting of middle Proterozoic crust due to magma underplating

Xingzhou Jiang [a], Zhiqiang Kang [a,b,*], Jifeng Xu [c], Zuohai Feng [a], Chongjin Pang [a], Guicong Fang [a], Jiachang Wu [a], Songquan Xiong [a]

[a] School of Earth Science and Guangxi Key Laboratory of Hidden Metallic Ore Deposit Exploration, Guilin University of Technology, Guilin 541004, China
[b] State Key Laboratory of Ore Geochemistry, Institute of Geochemistry, Chinese Academy of Sciences, Guiyang 550002, China
[c] Key Laboratory of Isotope Geochronology and Geochemistry, Guangzhou Institute of Geochemistry, Chinese Academy of Sciences, Guangzhou 510640, China

ARTICLE INFO

Article history:
Received 28 March 2016
Received in revised form 8 October 2016
Accepted 1 November 2016
Available online 2 November 2016

Keywords:
Granodiorite
Mafic microgranular enclave
Geochronology
Geochemistry
Tectonic setting
Shedong W–Mo ore district
Dayaoshan Uplift

ABSTRACT

The Shedong W–Mo ore district in the south–central Dayaoshan Uplift of Guangxi, southern China hosts the Baoshan and Pingtoubei deposits, both of which occur in granodioritic plutons. Zircon U–Pb dating of granodiorites and its mafic microgranular enclaves (MMEs) in the Baoshan deposit yielded ages of 439.8 ± 3.2 and 441.1 ± 2.2 Ma, respectively. Granodiorites have moderate SiO_2 (54.5–63.0 wt.%) and high Al_2O_3 (15.4–17.8 wt.%) contents, wide variations in major element ratios, significant rare earth element fractionation, and small negative Eu anomalies. They are rich in Th, U, Zr, and Hf, and depleted in Ba, Nb, and Ti. Their initial 87Sr/86Sr, $\varepsilon_{Nd}(t)$, and $\varepsilon_{Hf}(t)$ values are in the range of 0.7086–0.7091, −5.2 to −6.6 and −6.3 to +1.6, respectively. Rounded or lenticular MMEs have relatively low silica and high mafic components, depletion in Eu, Sr, and Zr, and marked negative Eu anomalies. Rb/Sr and Nb/Ta ratios, and $\varepsilon_{Nd}(t)$ and $\varepsilon_{Hf}(t)$ values of the MMEs are higher than those of host granodiorites, indicating a different magmatic source. Zircon U–Pb dating of the unexposed granodiorite porphyry in the Pingtoubei deposit yielded an age of 440.0 ± 1.7 Ma. The granodiorite porphyries have high SiO_2 and low K_2O, FeO^T, and MgO contents, with similar trace element features to the granodiorites at the Baoshan deposit, although the former has small negative Eu anomalies. Its initial 87Sr/86Sr values range from 0.7162 to 0.7173, $\varepsilon_{Nd}(t)$ values from −8.7 to −12.3, and $\varepsilon_{Hf}(t)$ values from −7.8 to +1.3, indicative of a crustal source. Nd and Hf two-stage model ages of the granodiorites, MMEs, and granodiorite porphyries have a narrow range between 1.3 and 2.2 Ga. We propose that the granodiorites and MMEs at the Baoshan deposit were produced through re-melting of middle Proterozoic crust as a result of underplating of mantle-derived magmas in a transitional compression-to-extension tectonic setting. Mantle-derived magmas provided the heat and material for the formation of the granodiorites and MMEs.

© 2016 Elsevier Ltd. All rights reserved.

1. Introduction

The Dayaoshan Uplift, located in the Guangxi Zhuang Autonomous Region is part of the NE-striking Qinzhou-Hangzhou metallogenic belt in southern China (Fig. 1a). The rocks in this region are mainly lower Paleozoic sedimentary rocks and minor plutonic rocks. Recent high-precision geochronological studies have reported that most of the granitoid plutons in this region were emplaced during the Early Paleozoic (430–470 Ma), Late Paleozoic to Early Mesozoic (240–270 Ma), and Late Mesozoic (150–170 and 90–110 Ma) (Chen et al., 2015). The Early Paleozoic and Late Mesozoic plutons are predominant in the Dayaoshan Uplift, which hosts a number of Cu–Au–W–Mo–(Ag) deposits. Previous studies showed that the mineralization occurred mainly during the Early Paleozoic and Late Mesozoic, and was closely related to intermediate-felsic granitoids (Cui et al., 2000; Liu and Cai, 2004; Zhong et al., 2010; Chen et al., 2011, 2015; Chen and Huang, 2012; Wei et al., 2012; Zhang et al., 2014).

The Shedong W–Mo ore district is located in the south–central Dayaoshan Uplift in Cangwu County. Previous studies have been carried out in the district to understand the regional tectonic evolution and the origins of ore fluids (Chen et al., 2011; Chen and

* Corresponding author at: School of Earth Science and Guangxi Key Laboratory of Hidden Metallic Ore Deposit Exploration, Guilin University of Technology, Guilin 541004, China.
E-mail address: zk99201@163.com (Z. Kang).

http://dx.doi.org/10.1016/j.jseaes.2016.11.004
1367-9120/© 2016 Elsevier Ltd. All rights reserved.

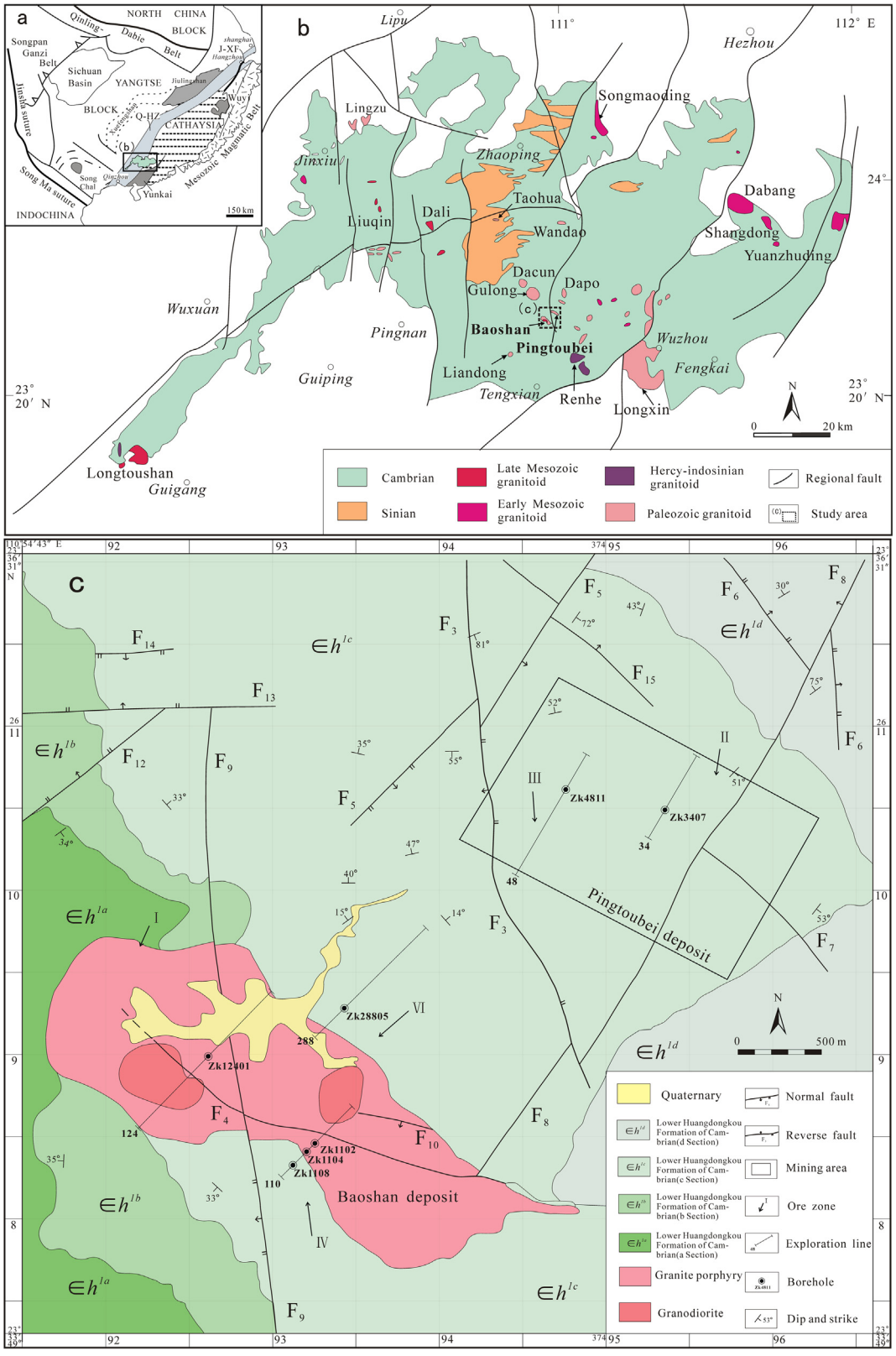

Fig. 1. (a) Tectonic sketch map of the South China Block (modified after Faure et al., 2009). (b) Sketch map of the Dayaoshan Uplift (modified after Chen et al., 2015). (c) Geological sketch map of the Shedong ore district (modified after Chen et al., 2012). Abbreviations are as follows: JLS: Neoproterozoic Jiulingshan Belt; XFS: Triassic Xuefengshan Belt; JSF: Jiangshan–Shaoxing Fault; Q–HZ: Qinzhou–Hangzhou Zone.

Huang, 2012; Zhang et al., 2014; Li et al., 2015). However, the petrogenesis and tectonic significance of Early Paleozoic granodioritic rocks remain poorly constrained. Some of these rocks contain abundant mafic microgranular enclaves (MMEs), particularly those formed by magma mingling. MMEs provide clues to the magma sources, petrogenetic histories, and deep magmatic processes of

granodioritic rocks (Vernon, 1983; Sunagawa, 1985; Castro and Moreno-ventas, 1991; Koyaguchi and Blake, 1991; Yang et al., 2007). In this study, we present systematic geochronological, geochemical, and isotopic study of the ore-forming granodioritic plutons and their MMEs from the Baoshan and Pingtoubei deposits in order to constrain their petrogenesis and tectonic setting of emplacement.

2. Geological setting

2.1. Regional geological setting

The Dayaoshan Uplift is an area of weakly metamorphosed basement composed mainly of Cambrian and minor Sinian strata. Both the Cambrian and Sinian sedimentary rocks are mainly flysch deposits with a total thickness of >9000 m, consisting of sandstone, siltstone, phyllite, and carbonaceous shale. E–W-striking faults and E–W-trending folds are well developed in the Dayaoshan Uplift, and form the Dayaoshan E–W-trending anticlinorium (Fig. 1b). The NE-striking, deep-seated Pingxiang–Dali Fault cuts across the Dayaoshan Uplift. A number of NE–SW- and N–S-striking faults are observed in this area. There are numerous intermediate–felsic batholiths, stocks, or pipes. These plutons are composed of granodiorite, granodiorite porphyry, monzogranite, and granite porphyry (Deng, 2012; Huang et al., 2013a,b). The Dayaoshan Uplift is also part of the NE–SW-striking Qinzhou–Hangzhou metallogenic belt (Yang and Mei, 1997; Yang et al., 2009).

2.2. Geology of the Shedong ore district

The Shedong W–Mo ore district comprises the Pingtoubei and Baoshan deposits (Fig. 1c). The lower Cambrian Huangdongkou Formation consists of neritic flyschand crops out in the ore district. This formation is composed of fine-grained sandstone and siltstone with interbedded shale and carbonaceous shale. Three groups of faults have been recognized in the district: (i) SE–NW-striking (faults F_4 and F_{10}), (ii) near N–S-striking (fault F_9), and (iii) NE–SW-striking (fault F_8). Based on field investigations, the SE–NW-striking faults are the earliest and the N–S-striking fault (F_9) is the youngest.

The granodiorite porphyry of the Pingtoubei deposit is strongly altered, and its surface exposure(veins) is only several meter-thick. The hidden part of the porphyry extends in the northwest direction and changes to an apophysis at deeper levels, where it is over 900 meter-long and 200–300 meter-thick. Significant quartz-vein-type W–Mo mineralization occurs within the pluton and its wall rock, forming the main mineralization zone (No. II and III ore zones) of the Shedong ore district. The Baoshan pluton is a small stock intruded into Cambrian strata and consists of granodiorite and granite porphyry. The pluton extends in a northwest direction and is 3 km-long and 1 km-wide. The granodiorite contains abundant MMEs, Quartz-vein-type scheelite mineralization and a small amount of molybdenite mineralization (No. I, IV, and VI ore zones). The granite porphyry has an intrusive contact with the granodiorite (Fig. 2a and b). Previous studies have reported ages for the granodiorite, granodiorite porphyry, and granite porphyry in the Shedong ore district range of 435.8–438.7 Ma, 432.0–438.1 Ma, and 91.1–94.8 Ma, respectively (Chen et al., 2011; Jiang et al., 2015; Li et al., 2015). A Re–Os isochron age of 437.8 ± 3.4 Ma has also been obtained on molybdenite related to the granodiorite porphyry at the Pingtoubei deposit (Chen et al., 2011), which is consistent with the zircon U–Pb age of the granodiorite porphyry. These data all suggest that W–Mo mineralization was formed in the Early Silurian.

3. Sampling

Samples of granodiorites from boreholes ZK1108, ZK28805, and ZK12401, and MMEs from boreholes ZK1102, ZK1104, and ZK1108 were collected from the Baoshan deposit. Samples of granodiorite porphyries from boreholes ZK3407 and ZK4811 were collected from the Pingtoubei deposit.

The granodiorite is grayish white and fine- to medium-grained, with a massive structure (Fig. 2c). It consists of plagioclase (40%), quartz (30–35%), hornblende, biotite, and minor K-feldspar. Plagioclase crystals are granular or short–prismatic in shape and generally 0.5–2.0 mm long, but up to 3 mm. Sericitization is generally developed within plagioclase. Quartz is granular and broadly the same size as the plagioclase. Biotite and hornblende (25–30%; Fig. 2d) range in size from 1 to 2 mm, although some crystals are up to 5 mm. The MMEs are black, fine-grained, rounded or lenticular in shape, 6–20 cm long (up to 50 cm), and typically exhibit sharp contacts with their host rocks and weak chilled margins. Some MMEs have marked reverse felsic veining (Fig. 2e and f). The MMEs are dominated by amphibole, plagioclase, biotite, and quartz, with subordinate apatite, zircon, and epidote (Fig. 2g and h). The apatite is acicular, indicating rapid cooling.

The granodiorite porphyry is dark gray in color and has a porphyraceous–porphyritic texture (Fig. 2i and j). The phenocryst minerals are mainly plagioclase (20%), quartz (10%), biotite, and amphibole (5%). Plagioclase crystals are granular or short–prismatic in shape, ranging from 1 to 2 mm in size. Some plagioclase crystals have undergone strong sericitization. Quartz crystals are granular and 2.0–3.5 mm in size. Biotite and hornblende are 2–3 mm in size, although some crystals are >5 mm. The matrix has an aphanitic texture and consists mainly of microcrystalline quartz and sericite. It is strongly silicified and contains visible pyrite (2%).

4. Analytical methods

4.1. Zircon U–Pb and Lu–Hf isotopic analyses

Zircons were separated using heavy liquid and magnetic techniques, and then purified by hand picking under a binocular microscope. Approximately 100–200 grains were randomly selected, mounted in epoxy and then polished to about half their thickness. Internal structures of the zircons were examined using cathodoluminescence (CL) imaging prior to isotopic analysis. U–Pb analyses were performed with a laser beam diameter of 35 μm by laser ablation–inductively coupled plasma–mass spectrometry (LA–ICP–MS) at the State Key Laboratory of Geological Processes and Mineral Resources, China University of Geosciences (GPMR-CUG), Wuhan, China. Detailed operating conditions for the laser ablation system, ICP–MS instrument, and data reduction are identical to those described by Liu et al. (2008, 2010). An Agilent 7500a ICP–MS instrument was used to acquire ion-signal intensities, coupled to a GeoLas 2005 laser ablation system. Helium was used as a carrier gas, and argon was used as the make-up gas and mixed with the carrier gas via a T-connector before entering the ICP–MS. Nitrogen was added into the central gas flow (Ar + He) of the Ar plasma to decrease the elemental detection limits and improve precision (Hu et al., 2008). Zircon 91500 was used as an external standard for U–Pb dating and analyzed twice every five analyses of the sample zircons. Time-dependent drift of U–Th–Pb isotopic ratios was corrected by linear interpolation (with time) for each set of five analyses according to the variations exhibited by zircon 91500 (Wiedenbeck et al., 1995). Preferred U–Th–Pb isotopic ratios used for 91500 were taken from Liu et al. (2010). The uncertainties of these preferred values for the external standard 91500 were propagated into the final results for the samples. Concordia diagrams

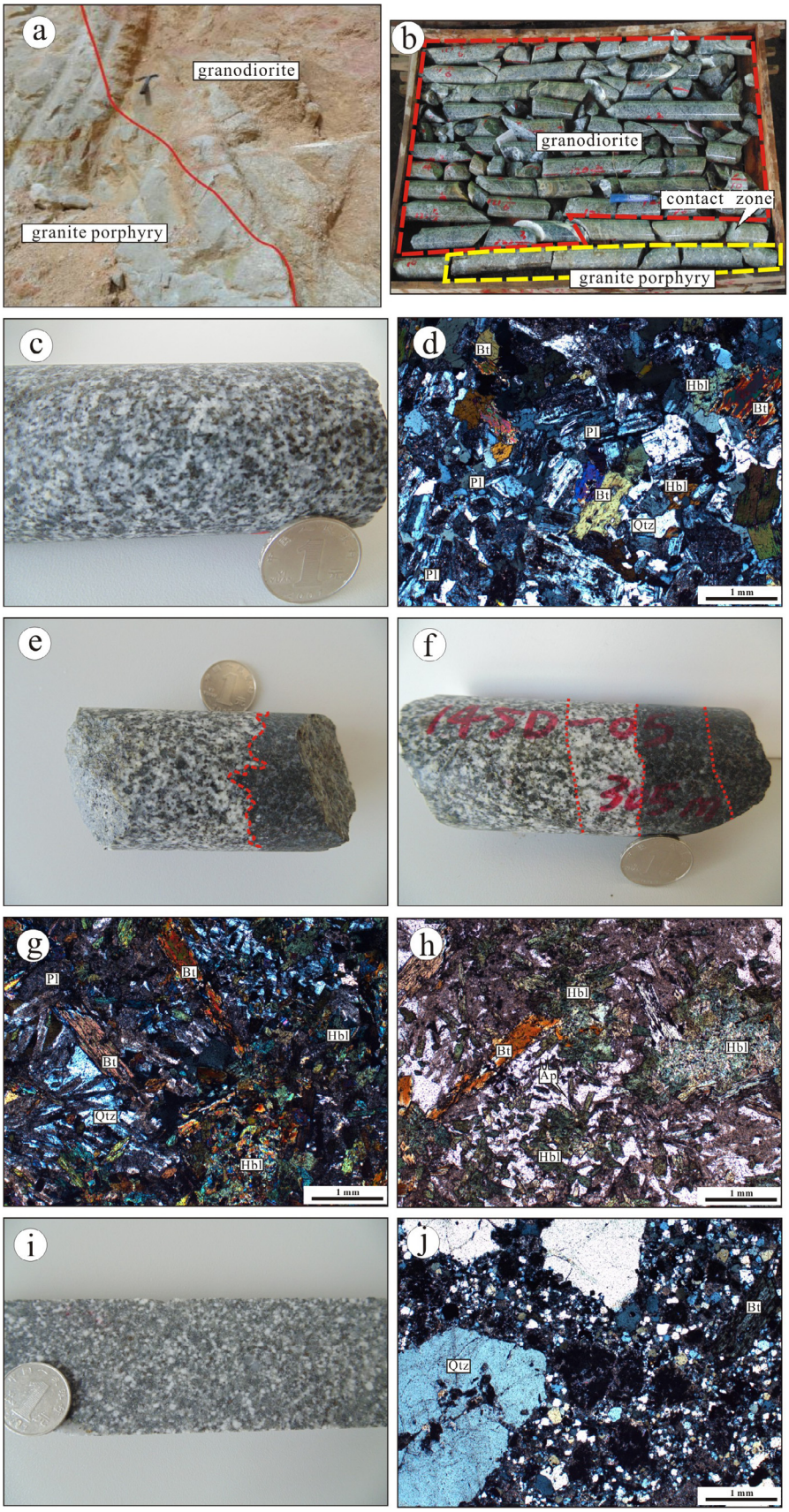

Fig. 2. Fieldphotographs showing: (a) contact relationship between granodiorite and granite porphyry; (b) sample from a borehole showing the contact relationship between granodiorite and granite porphyry; (c) granodiorite hand specimens from the borehole; (d) photomicrographs of the granodiorite (cross-polarized light); (e and f) contact relationship between granodiorite and MMEs; (g and h) representative photomicrographs of MMEs (g = cross-polarized light; h = plane-polarized light); (i) borehole sample; (j) petrographic characteristics of the granodiorite porphyry (cross-polarized light). Ap = Apatite; Bi = Biotite; Hbl = Hornblende; Plg = Plagioclase; Qtz = Quartz.

and weighted mean calculations were performed using Isoplot (V. 3.23) (Ludwig, 2003).

Insitu zircon Hf isotopic analyses were conducted on spots adjacent to where U–Pb age determinations were made. Hf isotopic compositions were determined with a Thermo Scientific Neptune Plus multiple-collector ICP–MS coupled to a New Wave UP193 solid-state laser ablation system at the State Key Laboratory for Mineral Deposits Research, Nanjing University, China. Zircons were ablated with a laser beam diameter of 32 or 44 μm, laser repetition rate of 8 Hz, and laser energy of 11.5–13.6 J/cm^2. During the Hf isotopic analyses, two reference standards were also analyzed, which were the 91500 zircon ($^{176}Hf/^{177}Hf = 0.282299 \pm 0.000017$; n = 14; 2σ) and Mud Tank zircon ($^{176}Hf/^{177}Hf = 0.282501 \pm 0.000006$; n = 26; 2σ). Measured $^{176}Hf/^{177}Hf$ ratios for these standards were within error (2σ) of their recommended values (Woodhead and Hergt, 2005; Griffin et al., 2007).

4.2. Whole-rock geochemical analyses

Rock samples were crushed into small chips and ultrasonically cleaned in distilled water and 5% HNO_3, then dried and handpicked to remove visible contamination. The rock chips were then ground to powder in an agate mill. The resulting powder was used for whole-rock major and trace element, and Sr–Nd isotope analyses at the Guangzhou Institute of Geochemistry, Chinese Academy of Sciences (GIGCAS), Guangzhou, China. Major elements were analyzed using a Rigaku RIX2000 X-ray fluorescence spectrometer (XRF), and analytical uncertainties are mostly between 1% and 5%. Trace element concentrations were obtained by ICP–MS after acid digestion of samples in high-pressure Teflon vessels. For details of the procedures for major and trace element analyses, see Liu et al. (1996) and Li et al. (2002, 2005).

Powdered samples were acid digested and subjected to Sr–Nd chemical separation at GIGCAS, and then the $^{87}Sr/^{86}Sr$ and $^{143}Nd/^{144}Nd$ ratios were measured with a MicromassIsoprobe multiple-collector ICP–MS at Guilin University of Technology, Guilin, China. Following the procedures described by Wei et al. (2002) and Li et al. (2004). Measured $^{87}Sr/^{86}Sr$ and $^{143}Nd/^{144}Nd$ ratios were normalized to $^{86}Sr/^{88}Sr = 0.1194$ and $^{146}Nd/^{144}Nd = 0.7219$, respectively. Reference standards were analyzed along with samples and yielded $^{87}Sr/^{86}Sr = 0.710269 \pm 16$ (2σ) for NBS987 and $^{143}Nd/^{144}Nd = 0.512089 \pm 8$ (2σ) for Shin Etsu JNDi-1, which are in good agreement with the recommended values of $^{87}Sr/^{86}Sr = 0.710248$ (McArthur, 1994) and $^{143}Nd/^{144}Nd = 0.512115 \pm 7$ (Tannaka et al., 2000), respectively.

Table 1
Zircon LA-ICP-MS U-Pb analyzing results for Shedong granodioritic rocks and MMEs (NO. 14SD-04, 14SD-05, 14SD-11).

Sample	Th	U	Th/U	$^{207}Pb/^{206}Pb$		$^{207}Pb/^{235}U$		$^{206}Pb/^{238}U$		$^{207}Pb/^{206}Pb$		$^{207}Pb/^{235}U$		$^{206}Pb/^{238}U$	
	$\times10^{-6}$			Ratio	±1σ	Ratio	±1σ	Ratio	±1σ	Age	±1σ	Age	±1σ	Age	±1σ
14SD-04-01	302	265	1.14	0.05611	0.00289	0.55025	0.02241	0.07066	0.00073	457	72	445	15	440	4
14SD-04-02	99	295	0.34	0.05617	0.00401	0.54896	0.02408	0.07060	0.00107	459	70	444	16	440	6
14SD-04-03	97	160	0.61	0.05680	0.00280	0.54333	0.04649	0.07059	0.00101	484	166	441	31	440	6
14SD-04-04	155	198	0.78	0.05733	0.00248	0.54714	0.02918	0.07057	0.00127	504	86	443	19	440	8
14SD-04-05	859	537	1.60	0.05816	0.00356	0.56634	0.01968	0.07046	0.00068	536	59	456	13	439	4
14SD-04-06	169	218	0.77	0.05247	0.00266	0.51043	0.02402	0.07043	0.00105	306	80	419	16	439	6
14SD-04-07	120	158	0.76	0.05859	0.00186	0.56052	0.03226	0.07041	0.00108	552	99	452	21	439	6
14SD-04-08	150	181	0.83	0.05700	0.00320	0.54827	0.02867	0.07062	0.00106	491	89	444	19	440	6
14SD-04-09	148	193	0.76	0.05700	0.00189	0.54190	0.03337	0.07024	0.00110	492	109	440	22	438	7
14SD-04-10	195	242	0.81	0.05887	0.00307	0.57200	0.02937	0.07130	0.00127	562	81	459	19	444	8
14SD-04-11	490	386	1.27	0.05630	0.00208	0.54517	0.01662	0.07067	0.00081	464	47	442	11	440	5
14SD-04-12	215	236	0.91	0.05916	0.00249	0.57056	0.02799	0.07128	0.00130	573	75	458	18	444	8
14SD-04-13	261	374	0.70	0.05638	0.00226	0.54671	0.02436	0.07039	0.00135	467	65	443	16	438	8
14SD-05-01	2821	1627	1.73	0.05545	0.00132	0.54379	0.01466	0.07051	0.00100	430	35	441	10	439	6
14SD-05-02	3371	2451	1.38	0.05397	0.00115	0.52993	0.01345	0.07057	0.00106	370	31	432	9	440	6
14SD-05-03	1124	904	1.24	0.0557	0.00149	0.54302	0.01379	0.07063	0.00075	440	37	440	9	440	5
14SD-05-04	1639	1417	1.16	0.05577	0.00138	0.54655	0.0134	0.07067	0.00069	443	37	443	9	440	4
14SD-05-05	1881	1371	1.37	0.05692	0.00162	0.55895	0.01696	0.07082	0.00108	488	41	451	11	441	6
14SD-05-06	4492	2633	1.71	0.05551	0.00119	0.54505	0.01371	0.07062	0.00101	433	31	442	9	440	6
14SD-05-07	3409	1968	1.73	0.05596	0.00129	0.5479	0.01634	0.07075	0.00152	451	32	444	11	441	9
14SD-05-08	2750	2625	1.05	0.05553	0.00114	0.54441	0.01366	0.07075	0.00124	434	28	441	9	441	7
14SD-05-09	1969	1618	1.22	0.05536	0.00129	0.54335	0.01241	0.07082	0.00068	427	34	441	8	441	4
14SD-05-10	1121	1012	1.11	0.05616	0.00164	0.55643	0.01689	0.07143	0.00096	459	43	449	11	445	6
14SD-05-11	937	952	0.98	0.05548	0.00144	0.54607	0.01414	0.07084	0.00066	431	41	442	9	441	4
14SD-05-12	2188	1604	1.36	0.05914	0.00168	0.58571	0.01893	0.07084	0.00102	572	45	468	12	441	6
14SD-05-13	2386	1644	1.45	0.05551	0.00157	0.54773	0.01589	0.07087	0.00074	433	46	444	10	441	4
14SD-05-14	1642	1530	1.07	0.05913	0.00148	0.58362	0.01568	0.07095	0.00088	572	37	467	10	442	5
14SD-05-15	1372	1337	1.03	0.0556	0.00143	0.55055	0.01425	0.07143	0.00077	437	38	445	9	445	5
14SD-05-16	1851	1692	1.09	0.05575	0.00127	0.54514	0.01236	0.07044	0.00051	443	37	442	8	439	3
14SD-05-17	2911	2176	1.34	0.05701	0.00116	0.56474	0.0144	0.07135	0.00117	492	29	455	9	444	7
14SD-05-18	1460	1349	1.08	0.05768	0.0014	0.56898	0.01392	0.07118	0.00065	518	38	457	9	443	4
14SD-11-01	1379	1815	0.76	0.05574	0.00125	0.54909	0.01292	0.07096	0.00096	442	29	444	8	442	6
14SD-11-02	443	658	0.67	0.05547	0.0015	0.54346	0.01462	0.07056	0.00068	431	43	441	10	440	4
14SD-11-03	3285	1096	3.00	0.05774	0.00153	0.56478	0.01538	0.07073	0.00081	520	40	455	10	441	5
14SD-11-04	218	376	0.58	0.05599	0.00206	0.54387	0.0189	0.07042	0.00095	452	53	441	12	439	6
14SD-11-05	664	834	0.80	0.05502	0.00151	0.54094	0.0146	0.07056	0.00057	413	46	439	10	440	3
14SD-11-06	843	1807	0.47	0.05535	0.00152	0.53773	0.01291	0.07054	0.0009	426	31	437	9	439	5
14SD-11-07	1066	1219	0.87	0.05513	0.00110	0.53647	0.01094	0.07066	0.00020	417	44	436	7	440	1
14SD-11-08	968	742	1.31	0.06303	0.00133	0.61612	0.01316	0.07092	0.00015	709	44	487	8	442	1
14SD-11-09	833	917	0.91	0.06036	0.00084	0.58817	0.00866	0.07063	0.00029	617	34	470	6	440	2
14SD-11-10	1907	2478	0.77	0.05855	0.00059	0.56871	0.00564	0.07063	0.00035	550	22	457	4	440	2
14SD-11-11	2744	1711	1.60	0.05665	0.00054	0.55137	0.00559	0.07070	0.00042	480	20	446	4	440	3

5. Analytical results

5.1. Zircon U–Pb ages

Zircon U–Pb isotopic data for samples 14SD-04 (granodiorite), 14SD-11 (granodiorite porphyry), and 14SD-05 (MME) are presented in Table 1. Zircon grains from samples 14SD-04 and 14SD-11 are mostly granular or prismatic, and 100–250 μm in length, and have length-to-width ratios of 1:1–5:1. The zircons show obvious magmatic oscillatory zoning. Twenty-four analyses of 24 zircon grains from sample 14SD-04 were carried out. After excluding discordant and inherited ages, 13 grains were plotted on a U–Pb concordia diagram, yielding a weighted mean $^{206}Pb/^{238}U$ age of 439.8 ± 3.2 Ma (MSWD = 0.1) (Fig. 3a and d). Twenty-four analyses of 24 zircon grains from sample 14SD-11 were conducted, among which 11 grains yielded concordant $^{206}Pb/^{238}U$ ages with a weighted mean age of 440.0 ± 1.7 Ma (MSWD = 0.08) (Fig. 3b and e). These results indicate that the granodiorite and granodiorite porphyry of the Shedong ore district formed in the Early Silurian.

Zircon grains from MMEs (sample 14SD-05) are mostly short–prismatic or granular, and smaller and darker than the zircon grains in host granodiorites. These zircons are 50–130 μm in length and have length-to-width ratios of 1:1–2.5:1. Twenty-four analyses of 24 zircon grains with obvious magmatic oscillatory zoning from sample 14SD-05 were analyzed, among which 18 grains yielded concordant $^{206}Pb/^{238}U$ ages with a weighted mean age of 441.1 ± 2.2 Ma (MSWD = 0.13) (Fig. 3c and f), which is interpreted to be the formation age of the MMEs. This age is within error of the age of host granodiorites.

5.2. Whole-rock geochemistry

Geochemical data for granodioritic rocks and MMEs from the Shedong W–Mo ore district are listed in Table 2. The granodiorite has variable SiO_2 (54.5–63.0 wt.%), high Al_2O_3(15.4–17.8 wt.%), FeO^T(5.8–7.9 wt.%), MgO(3.0–4.3 wt.%) and CaO(4.5–8.3 wt.%) contents, high $Mg^{\#}$ values (49.5–55.8), and low alkali contents. On a SiO_2 vs. $Na_2O + K_2O$ (TAS) diagram (Fig. 4a), data for the samples plot mainly in the diorite–granodiorite fields. Compared with the granodiorites, the granodiorite porphyries have higher SiO_2 (66.0–70.4 wt.%), and lower FeO^T(3.0–4.4 wt.%) and MgO(1.2–1.9 wt.%) contents. On a TAS diagram, data for the samples plot mainly in the subalkaline granodiorite field (Fig. 4a). On a SiO_2 vs. K_2O diagram, both the granodiorites and granodiorite porphyries are classified mainly as medium-K rocks (Fig. 4b). In an A/CNK vs. A/NK diagram, data for the granodiorite samples fall mostly in the subalkaline–metaluminous field, whereas data for the granodiorite porphyries plot in the weakly peraluminous field (Fig. 4c). The MMEs have lower SiO_2 contents (52.5–58.7 wt.%), and higher FeO^T(9.2–11.9 wt.%), MgO(4.7–6.6 wt.%), and K_2O(2.0–3.4 wt.%) contents than those of host rocks. Data for the MMEs plot in the syenodiorite–diorite field on a TAS diagram, and in the high-K calc-alkaline to shoshonitic series on a SiO_2 vs. K_2O diagram (Fig. 4a and b).

The samples have variable total rare earth element (REE) contents. The MMEs, granodiorites, and granodiorite porphyries have average $(La/Yb)_N$ ratios of 2.21, 4.69, and 10.72, respectively, showing increasing light to heavy REE fractionation. The granodiorites and granodiorite porphyries have similar REE patterns (Fig. 5a and b), showing light REE enrichment with small negative Eu anomalies. The negative Eu anomalies of the granodiorites (average δEu = 0.28) are more prominent than those of the granodiorite porphyries. The MMEs have relatively flat REE patterns with a significant negative Eu anomaly (0.18) and no prominent light to heavy REE fractionation (Fig. 5c). In primitive-mantle-normalized multi-element patterns, most granodiorite samples have similar features to those of the granodiorite porphyry, exhibiting enrichment in U and Th, and depletion in Nb, Ta, Ti, and the large-ion lithophile element (LILE). However, other samples have similar patterns to the MMEs and do not have negative Ta anomalies (Fig. 5d–f). Primitive mantle-normalized multi-element patterns for the MMEs are more complicated, showing significant negative Nb, Ti, Sr, Zr, and Eu anomalies.

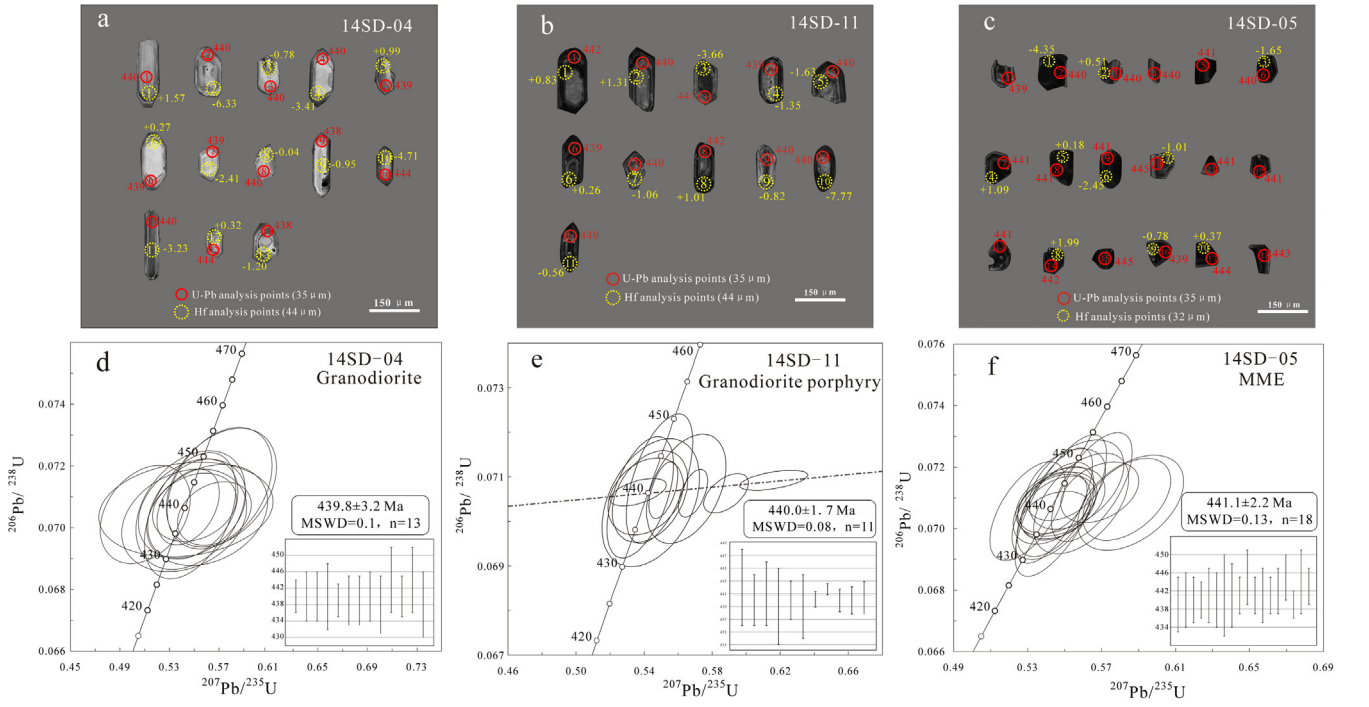

Fig. 3. Cathodoluminescence (CL) images of zircon grains (a–c) and U–Pb concordia diagrams (d–f) for granodioritic rocks and MMEs from the Shedong ore district. (a and d) 14SD-04-granodiorite; (b and e) 14SD-11-granodiorite porphyry; (c and f) 14SD-05-MMEs.

Table 2
Analytical results of the major elements (wt.%) and trace elements ($\times 10^{-6}$) for granodioritic rocks and MMEs from Shedong ore district.

Sample	Granodiorite					MME					Granodiorite porphyry					
	14SD-02	14SD-03	14SD-04	14SD-07	13BS-5-2	14SD-05-1	14SD-05-2	ZK1102-37	ZK1104-64	ZK1104-67	13BS-4	13PTB-7	14SD-11	14SD-12	14SD-13	14SD-14
Depth	ZK1108 255 m	ZK1108 245 m	ZK1108 299 m	ZK1108 167 m	ZK28805 599 m	ZK1108 305 m	ZK1108 340 m	ZK1102 103 m	ZK1104 144 m	ZK1104 153 m	ZK12401 105 m	ZK4811 910 m	ZK3407 212 m	ZK3407 227 m	ZK3407 305 m	ZK3407 287 m
Major oxides (wt.%)																
SiO_2	55.41	54.48	61.29	55.73	63.00	55.86	53.08	58.67	52.74	52.47	70.08	68.30	67.81	66.04	70.36	68.31
TiO_2	0.57	0.56	0.49	0.52	0.50	0.68	0.55	0.55	0.51	0.61	0.27	0.21	0.51	0.25	0.24	0.24
Al_2O_3	17.82	17.65	15.82	17.09	15.40	12.83	15.00	15.94	14.69	16.70	14.83	15.55	14.76	15.54	14.03	15.08
$Fe_2O_3^T$	8.21	8.56	7.33	8.21	6.30	10.61	10.40	9.89	10.38	12.77	3.22	3.35	4.51	4.82	3.50	3.93
MnO	0.17	0.19	0.18	0.16	0.13	0.31	0.31	0.17	0.31	0.25	0.07	0.10	0.10	0.11	0.09	0.08
MgO	4.19	4.22	3.09	4.29	2.97	6.57	5.81	4.67	6.04	6.14	1.39	1.30	1.91	1.74	1.20	1.43
CaO	7.81	8.35	5.45	8.08	4.53	6.39	7.07	0.41	7.23	2.85	1.50	3.52	2.21	4.34	2.89	4.06
Na_2O	2.73	2.71	2.78	2.30	2.56	2.25	2.79	3.34	2.84	2.15	3.56	3.25	3.04	3.33	3.04	3.11
K_2O	1.44	1.42	1.95	1.60	2.80	2.04	3.38	2.94	3.16	2.22	2.82	2.64	3.40	1.69	2.89	1.34
P_2O_5	0.17	0.19	0.15	0.14	0.06	0.31	0.11	0.12	0.10	0.13	0.03	0.04	0.03	0.09	0.07	0.09
LOI	1.40	1.36	1.23	1.32	1.57	2.06	1.16	3.54	1.77	3.96	1.69	1.35	1.80	1.68	1.72	1.87
Total	99.92	99.67	99.75	99.44	99.82	99.91	99.67	100.25	99.78	100.26	99.47	99.61	100.08	99.64	100.02	99.54
FeO^T	7.50	7.88	6.70	7.43	5.77	9.76	9.50	9.20	9.53	11.9	2.96	3.06	4.13	4.43	3.20	3.62
K_2O/Na_2O	0.53	0.52	0.70	0.70	1.09	0.91	1.21	0.88	1.11	1.03	0.79	0.81	1.12	0.51	0.95	0.43
Mg#	54.3	53.4	49.5	55.8	52.4	59.1	56.5	52.4	57.6	52.8	50.2	47.4	49.7	45.7	44.4	46.0
Trace element ($\times 10^{-6}$)																
Sc	26.43	26.18	19.96	26.73	21.87	27.34	51.74	41.17	49.06	44.57	9.26	7.83	12.64	8.57	7.56	7.40
Ti	3337.20	3350.00	2919.30	3179.70	3090.30	4088.70	3346.30	3078.30	3089.50	3472.40	1500.7	1227.80	3058.60	1367.80	1479.60	1365.10
V	203.60	218.70	157.50	214.80	147.90	205.00	319.20	224.50	270.70	364.20	64.04	69.15	84.41	48.87	58.85	65.84
Cr	48.70	55.39	40.71	36.73	23.59	299.50	116.40	125.80	152.50	136.70	16.79	25.26	60.13	18.28	18.32	13.79
Mn	1304.40	1447.00	1316.10	1236.00	1023.40	2322.30	2416.30	1194.70	2383.00	1807.00	531.70	726.20	732.50	840.20	657.30	576.50
Co	21.62	22.65	16.79	23.73	15.77	26.38	27.11	36.88	27.97	19.27	6.82	10.60	8.23	11.48	6.12	6.75
Ni	20.49	21.88	15.82	21.77	12.07	88.87	28.98	25.33	31.79	27.17	6.91	9.67	28.91	6.99	9.47	6.25
Cu	66.75	49.60	119.00	50.20	56.17	28.80	264.50	198.10	283.20	140.90	17.75	124.60	58.69	300.90	188.40	189.00
Zn	111.60	83.45	206.30	74.96	69.66	135.60	104.80	86.54	108.90	197.60	42.33	53.26	52.05	44.92	44.49	42.42
Ga	19.11	18.97	17.63	17.52	15.91	16.89	17.77	17.55	18.10	23.97	14.00	15.38	15.95	14.31	14.20	15.48
Ge	2.42	2.49	2.34	2.22	1.95	3.43	3.15	2.22	3.19	3.14	1.31	1.75	1.89	1.59	1.43	1.44
Rb	86.79	71.32	159.40	73.44	129.50	194.60	126.90	175.30	150.60	161.80	139.20	132.60	190.40	104.10	129.80	91.73
Sr	342.70	329.40	271.40	261.70	199.30	172.40	164.80	62.31	200.10	202.90	137.60	247.10	186.70	261.30	224.20	258.20
Y	25.30	23.79	26.20	19.44	25.81	36.14	63.23	26.90	53.07	29.12	11.80	7.91	26.45	9.14	17.79	12.81
Zr	77.28	119.40	135.40	96.76	206.80	161.20	48.77	67.02	33.39	89.80	111.80	111.50	161.10	94.08	101.60	101.00
Nb	6.17	6.20	8.62	5.51	9.61	13.15	11.85	15.00	11.96	12.06	7.81	10.52	14.77	8.55	7.76	7.78
Cs	7.48	5.60	12.64	4.70	7.86	8.28	3.90	7.22	5.64	7.87	9.04	8.73	9.35	8.18	4.22	3.74
Ba	397.30	417.50	544.90	511.70	777.20	479.10	987.80	481.10	602.20	660.30	576.90	742.20	1506.20	658.40	806.60	354.50
La	16.51	23.81	9.15	17.51	12.30	18.44	6.84	13.07	8.60	11.46	10.43	14.34	36.61	24.19	22.23	26.74
Ce	36.43	49.57	22.07	34.24	26.39	50.35	24.61	29.52	27.72	31.86	18.52	25.38	71.00	43.24	41.57	50.23
Pr	4.90	6.00	3.31	4.10	3.53	7.81	4.71	3.90	4.93	5.01	2.00	2.70	8.16	4.62	4.67	5.40
Nd	20.14	22.52	14.77	15.72	14.69	32.95	24.61	16.68	24.14	22.29	6.86	8.93	29.73	15.25	16.57	18.45
Sm	4.18	4.17	3.64	3.13	3.49	6.39	7.51	3.81	6.74	5.29	1.32	1.47	5.47	2.34	2.99	2.96
Eu	0.97	0.99	0.84	0.78	0.76	1.23	1.30	0.59	1.16	0.63	0.33	0.51	1.12	0.62	0.73	0.67
Gd	3.85	3.86	3.56	3.03	3.46	5.28	7.80	3.49	6.73	4.85	1.38	1.33	4.79	1.99	2.73	2.43
Tb	0.67	0.63	0.67	0.51	0.67	0.88	1.53	0.61	1.31	0.86	0.27	0.21	0.75	0.28	0.45	0.36
Dy	4.20	3.89	4.13	3.22	4.10	5.52	9.99	3.94	8.41	5.10	1.74	1.21	4.45	1.50	2.79	2.10
Ho	0.90	0.84	0.93	0.70	0.92	1.19	2.17	0.88	1.85	1.04	0.41	0.28	0.93	0.32	0.60	0.45
Er	2.57	2.42	2.71	2.01	2.75	3.64	6.34	2.72	5.37	2.83	1.29	0.82	2.64	0.94	1.82	1.29
Tm	0.39	0.37	0.42	0.30	0.43	0.59	0.98	0.45	0.85	0.41	0.21	0.13	0.41	0.15	0.29	0.20
Yb	2.50	2.43	2.79	2.00	2.84	4.15	6.41	3.23	5.61	2.64	1.50	0.91	2.65	1.07	1.97	1.40
Lu	0.39	0.39	0.46	0.32	0.49	0.69	0.99	0.55	0.88	0.44	0.26	0.17	0.42	0.19	0.31	0.24
Hf	2.53	3.36	4.07	3.00	5.82	4.87	2.57	3.76	2.17	3.51	3.69	3.55	4.50	2.81	3.24	3.13

(*continued on next page*)

Table 2 (*continued*)

Sample	Granodiorite					MME			Granodiorite porphyry						
	14SD-02	14SD-03	14SD-04	14SD-07	13BS-5-2	14SD-05-1	14SD-05-2	ZK1102-37	ZK1104-64	ZK1104-67	13BS-4	13PTB-7	14SD-11	14SD-12	14SD-13	14SD-14
Ta	0.46	0.46	0.69	0.47	0.81	1.26	0.95	1.10	0.82	0.83	1.07	1.00	1.42	0.82	0.82	0.70
Th	5.51	8.28	5.75	9.15	7.65	14.42	4.78	9.60	7.15	8.87	12.49	17.16	20.10	19.99	17.35	18.27
U	1.39	1.72	2.78	1.72	3.49	4.80	4.68	9.76	5.52	5.10	4.52	6.78	2.94	2.11	8.26	4.86
∑REE	98.60	121.89	69.45	87.56	76.82	139.11	105.79	83.43	104.29	94.70	46.50	58.37	169.13	96.70	99.72	112.92
δEu	0.25	0.25	0.28	0.33	0.29	0.17	0.13	0.27	0.15	0.20	0.74	0.72	0.20	0.46	0.35	0.37
$(La/Yb)_N$	4.73	7.02	2.35	6.27	3.10	3.18	0.77	2.90	1.10	3.12	4.98	11.35	9.91	16.22	8.09	13.74
Rb/Sr	0.25	0.22	0.59	0.28	0.65	1.13	0.77	2.81	0.75	0.80	1.01	0.54	1.02	0.40	0.58	0.36
Nb/Ta	13.41	13.48	12.49	11.72	11.86	10.44	12.47	13.64	14.59	14.53	7.30	10.52	10.40	10.43	9.46	11.11
Rb/Nb	14.07	11.50	18.49	13.33	13.48	14.80	10.71	11.69	12.59	13.42	17.82	12.60	12.89	12.18	16.73	11.79

The Cr, Ni, V, and Co concentrations of the MMEs are the highest, followed by the granodiorites and then the granodiorite porphyries. Average Rb/Sr (0.40, 1.25, and 0.65) and Rb/Nb ratios (14.17, 12.64, and 14.00) of the granodiorites, MMEs, and granodiorite porphyries are higher than average upper crustal values in central China (average Rb/Sr = 0.31; average Rb/Nb = 6.80) and globally (average Rb/Sr = 0.32; average Rb/Nb = 4.50). Nb/Ta ratios of the MMEs (average = 13.13) approach the values for primitive mantle (17.80); the granodiorites (11.71) and granodiorite porphyries (10.38) have lower values. In general, the trace element systematics of the granodiorites are intermediate between those of the granodiorite porphyries and MMEs, but closer to those of the granodiorite porphyries.

5.3. Sr–Nd–Hf isotopes

The $\varepsilon_{Nd}(t)$ values of the MMEs (−5.1 to −6.0) are similar to those of the host granodiorites (−5.2 to −6.6), but different from those of the granodiorite porphyries (−8.7 to −12.3). The initial $^{87}Sr/^{86}Sr$ ratios of the MMEs vary considerably from 0.7032 to 0.7117. The initial $^{87}Sr/^{86}Sr$ ratios of the granodiorites and granodiorite porphyries are 0.7086–0.7091 and 0.7162–0.7173, respectively. Two-stage Nd isotope model ages of the granodiorites, granodiorite porphyries, and MMEs are all concentrated between 1.6 and 2.2 Ga (Table 3).

Zircon $^{176}Lu/^{177}Hf$ ratios are less than 0.002, indicating that after zircon formation there was little accumulation of radiogenic Hf. Thus, the measured $^{176}Hf/^{177}Hf$ ratios can be used to represent $^{176}Hf/^{177}Hf$ ratios during crystallization (Wu et al., 2007a). The zircon $\varepsilon_{Hf}(t)$ values of the granodiorites, granodiorite porphyries, and MMEs are −6.3 to +1.6, −7.8 to +1.3, and −4.3 to +2.0, respectively. Such variations are much larger than analytical uncertainties, indicating that these samples have heterogeneous zircon Hf isotopic compositions. Correspondingly, the two-stage Hf isotope model ages of the samples vary between 1.3 and 1.9 Ga, which are slightly younger than the whole-rock, two-stage Nd isotope model ages (Table 4).

6. Discussion

6.1. Petrogenesis

6.1.1. I-type granodiorite

The granodioritic rocks in the Shedong ore district contain few melanocratic, K-rich mafic minerals. Zircon saturation temperatures are 578–795 °C, indicating a low formation temperature (Watson and Harrison, 1983). The ratio of 10,000 × Ga/Al is less than 2.6, suggesting that the granodioritic rocks are not A-type granites. Euhedral–subhedral hornblende is present in the granodiorite samples (Fig. 2d). A/CNK values of most samples are less than 1.1, and the samples plot within the metaluminous to weakly peraluminous fields (Fig. 4c) on an A/CNK vs. A/NK diagram, showing an I-type granite affinity (Chappell and White, 1974). P_2O_5, Th, and Rb are reliable indicators for distinguishing I-and S-type granites (Chappell and White, 1992; Wu et al., 2007b). On diagrams of SiO_2 vs. P_2O_5 and A/CNK vs. P_2O_5 (Fig. 6a and b), data for the samples all show evolutionary trends typical of I-type granitoids.

6.1.2. Mingling of magmas from different sources

Minerals in the MMEs are euhedral–subhedral and much smaller than those in the host granodiorites. The MMEs have sharp boundaries with their host granodiorites and exhibit a gray–black chilled rim (Fig. 2f). Acicular apatite is well developed, indicating rapid cooling and crystallization of the mafic magmas (Wyllie et al., 1962). Felsic veins occur at the rims of MMEs as a result of

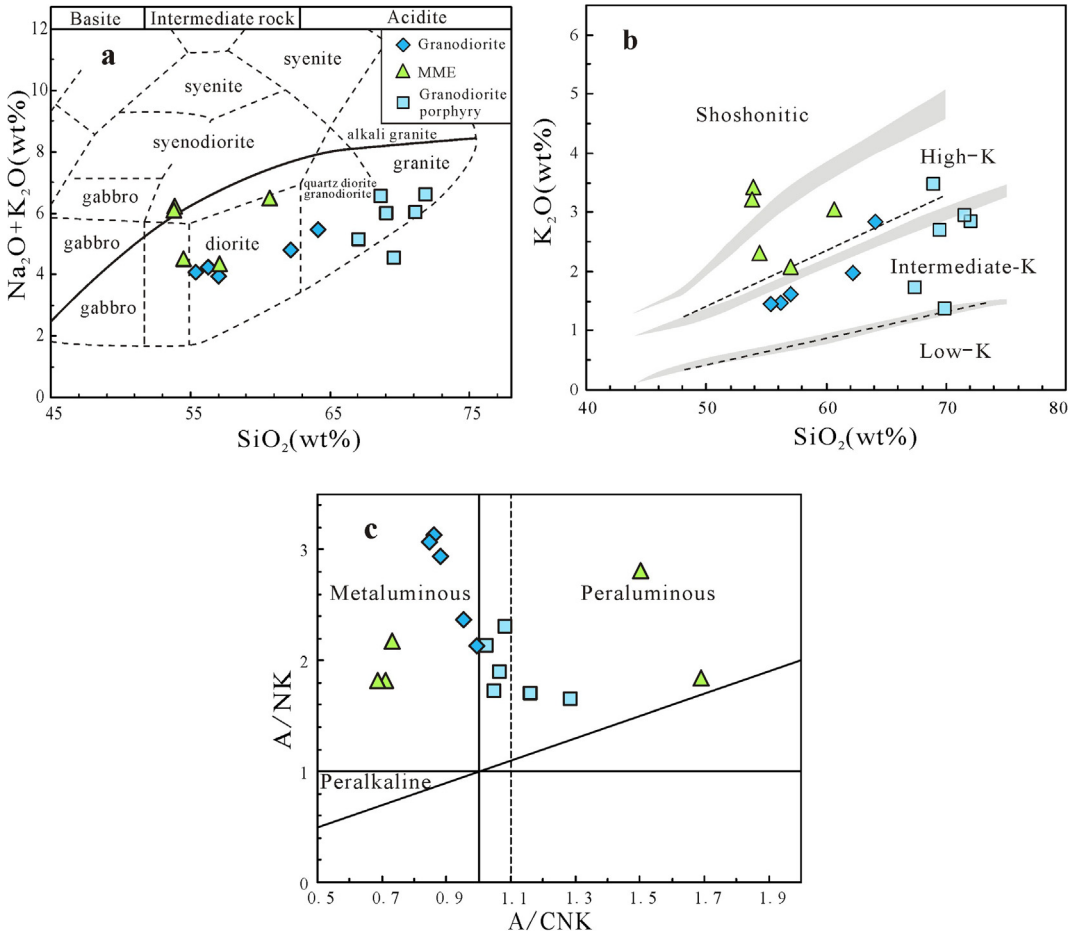

Fig. 4. Geochemical discrimination diagrams for the granodioritic rocks and MMEs from the Shedong ore district. (a) TAS diagram after Wilson (1989); (b) SiO_2 vs. K_2O diagram after Peccerillo and Taylor (1976); (c) A/CNK vs. A/NK diagram after Middlemost (1985) and Maniar and Piccoli (1989), where A/CNK = Al_2O_3 (molar)/(K_2O + Na_2O + CaO) (molar) and A/NK = Al_2O_3 (molar)/(Na_2O + K_2O) (molar).

the following processes: (1) rapid cooling and chilling of mafic magmas that led to cracks forming on the rims of MMEs; and (2) the influence of the hot mafic magma meant that the viscosity of the granitic magmas decreased, causing felsic minerals to aggregate at the contact between the two types of magma or penetrate into the cracks (Zhu et al., 2006) (Fig. 2e).

LA–ICP–MS zircon U–Pb ages of the present study indicate that the granitoids of the Shedong ore district formed coevally at ca. 440 Ma, and these ages are consistent with previously published results (Chen et al., 2011; Li et al., 2015). However, the granitoids show significantly different geochemical characteristics, such as the variable SiO_2 and K_2O contents of the granodiorites, and relatively high $Mg^{\#}$ values and MgO, FeO^T, and CaO contents compared with those of the granodiorite porphyries. The granodiorite porphyries have similar characteristics to crustal sources (high SiO_2, but low K_2O, MgO, FeO_T, and CaO). Both the granodiorites and granodiorite porphyries belong to the metaluminous to weakly peraluminous calc-alkaline I-type granite series. Such granitoids have been interpreted to result from re-melting of the upper crust as a result of underplating of mantle-derived magmas, with input of mantle materials during their formation (Kemp et al., 2005, 2007; Wang et al., 2007; Zhu et al., 2009; He et al., 2010; Lou et al., 2010; Xie et al., 2013; Wang, 2014).

Compared with the granodiorites and granodiorite porphyries, the MMEs within the granodiorites of the Shedong ore district have lower SiO_2 contents, higher FeO^T, MgO, and CaO contents, and higher $Mg^{\#}$, Cr, and Ni values. Nb/Ta ratios (up to 14.5) are close to that of primitive mantle (17.5) (McDonough and Sun, 1995). On a Cr/Zr vs. Th/Sc diagram (Fig. 7a), data for the granodiorites are intermediate between those of the granodiorite porphyries and MMEs. On SiO_2/MgO vs. Al_2O_3/MgO and MgO vs. FeO^T diagrams (Fig. 7b and c), the samples show an obvious magmatic mingling trend, indicating that they formed by mixing of magmas from different sources (Nitoi et al., 2002; Perugini et al., 2003). Incontrast, there is no obvious fractional crystallization trend in a Rb vs. Ba diagram, indicating that fractional crystallization had little effect on magma genesis (Fig. 7d).

The zircon $\varepsilon_{Hf}(t)$ values of the granodiorites, granodiorite porphyries, and MMEs are −6.3 to +1.6, −7.8 to +1.3, and −4.3 to +2.0, respectively. The two-stage Hf isotope model ages of these samples are between 1.3 and 1.9 Ga (Fig. 8a; Table 4), indicating they formed by re-melting of middle Proterozoic crust with input of mantle material. In addition, the $\varepsilon_{Hf}(t)$ values of the samples vary significantly (6-9ε units), which is more variable than observed in previous studies ($\varepsilon_{Hf}(t)$ = −3.7 to 0.0; Li et al., 2015). Given that zircon Hf isotopes cannot be changed by fractional crystallization or partial melting (Bolhar et al., 2008), such zircon Hf isotope variations have been interpreted to result from magma mingling between mantle- and crust-derived magmas (Griffin et al., 2002; Beloisova et al., 2006; Kemp et al., 2007; Yang et al., 2007). On an I(Sr) vs. $\varepsilon_{Nd}(t)$ diagram (Fig. 8b), data for the granodiorites and MME samples plot near data for Early Paleozoic gabbros and S-type granites and paragneisses in southern China (ca. 434 Ma) excepted for one sample of the MMEs, which showed a

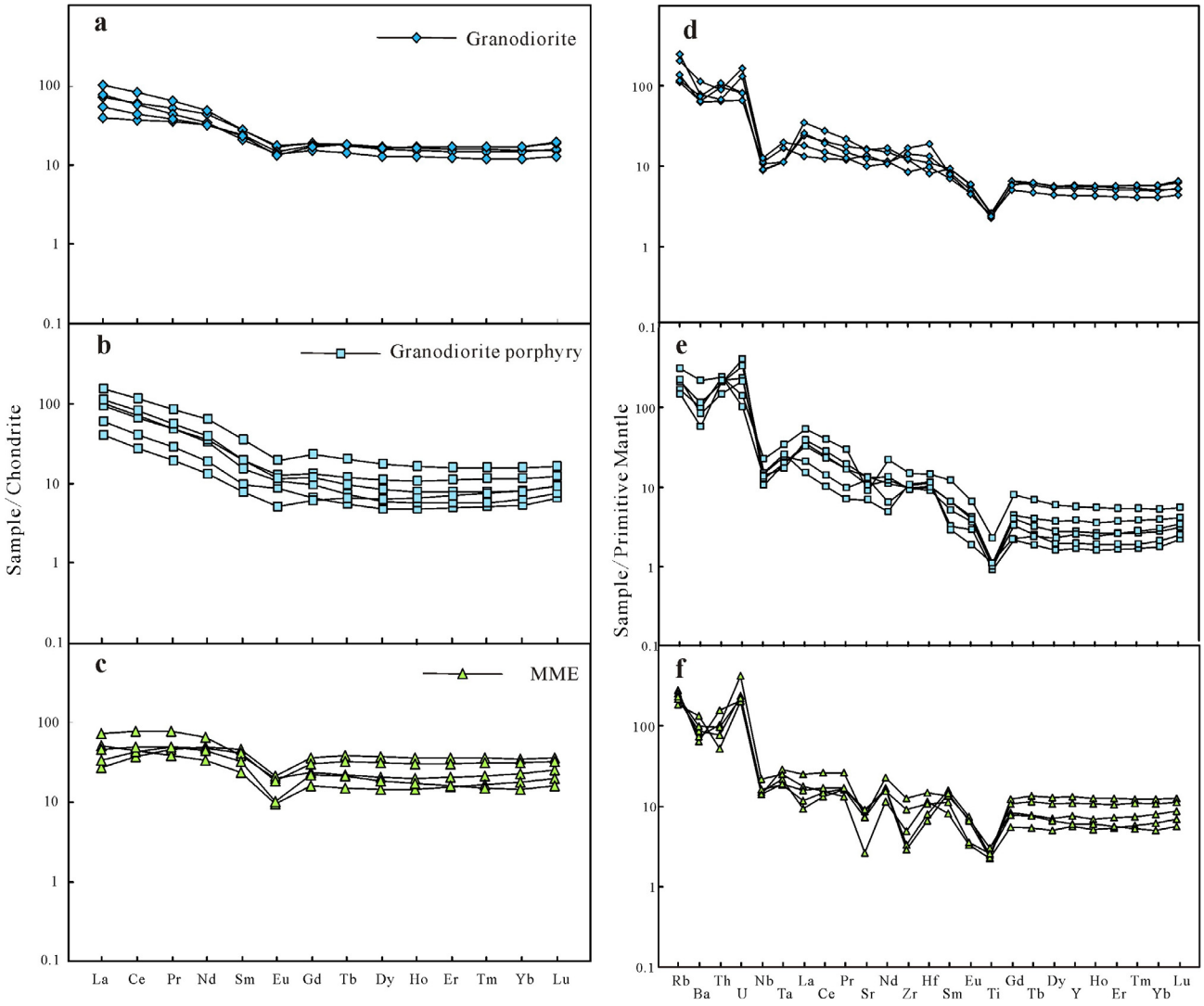

Fig. 5. Chondrite-normalized REE (a–c) and primitive-mantle-normalized trace element patterns (d–f) for granodioritic rocks and MMEs from the Shedong ore district. Normalizing values for chondrite and primitive mantle are from McDonough and Sun (1995).

Table 3
Sr and Nd isotopic compositions for the Shedong granodioritic rocks and MMEs.

Sample	Granodiorite		MME			Granodiorite porphyry	
	14SD-04	14SD-07	14SD-05-1-1	14SD-05-1-2	ZK1104-67	14SD-11	14SD-13
Depth	ZK1108 299 m	ZK1108 167 m	ZK1108 305 m	ZK1108 306 m	ZK1104 144 m	ZK3407 212 m	ZK3407 305 m
$^{87}Rb/^{86}Sr$	1.6995	0.8120	3.2662	3.2662	2.3075	2.9509	1.6752
$^{87}Sr/^{86}Sr$	0.719206	0.714234	0.732191	0.723692	0.724245	0.735809	0.726737
2σ	9	7	7	5	8	7	8
$(^{87}Sr/^{86}Sr)i$	0.7086	0.7091	0.7117	0.7032	0.7098	0.7173	0.7162
$^{147}Sm/^{144}Nd$	0.1488	0.1537	0.1171	0.1171	0.1434	0.1112	0.1091
$^{143}Nd/^{144}Nd$	0.512232	0.512178	0.512101	0.512106	0.512221	0.511763	0.511939
2σ	4	4	4	4	4	4	4
$\varepsilon_{Nd}(t)$	−5.2	−6.6	−6.0	−5.9	−5.1	−12.3	−8.7
T_{DM2}	1.60	1.71	1.67	1.66	1.60	2.17	1.89

quite large deviation of $^{87}Sr/^{86}Sr$. However, its ε_{Nd} (t) value is identical to those of other samples. Therefore, such a deviation of Sr isotopic composition of this sample may resulted from the influence of ore fluids. Data for the granodiorite porphyries fall within the field for continental lithologies, but with a wider range than the granodiorites. In summary, it is likely that the granodioritic rocks of the Shedong ore district formed by varying degrees of magma mingling between magmas derived from the crust and mantle.

6.2. Tectonic setting

Early Paleozoic tectonic setting of the South China Block are debated. The current hypotheses as to the tectonic setting are that it was: (1) an ocean-to-continent subduction system, related to a collisional orogeny (e.g., Guo et al., 1984; Peng et al., 2006); and (2) an intra-continental orogeny (e.g., Ren et al., 1980; Ren, 1990). Although most studies prefer the second option, the trans-

Table 4
Zircon Hf isotopic compositions for the Shedong granodioritic rocks and MMEs.

No.	$^{176}Hf/^{177}Hf$	2σ	$^{176}Lu/^{177}Hf$	2σ	$^{176}Yb/^{177}Hf$	2σ	T(Ma)	T_{DM1}(Ga)	T_{DM2}(Ga)	$(^{176}Hf/^{177}Hf)_i$	$\varepsilon_{Hf}(t)$
Granodiorite											
1	0.282548	0.000025	0.000624	0.000003	0.014710	0.000072	440	0.99	1.32	0.28254	1.57
2	0.282326	0.000028	0.000841	0.000028	0.021979	0.000783	440	1.30	1.82	0.28232	−6.33
3	0.282487	0.000030	0.001275	0.000022	0.030115	0.000542	440	1.09	1.47	0.28248	−0.78
4	0.282416	0.000030	0.001677	0.000023	0.044039	0.000639	440	1.20	1.63	0.2824	−3.41
5	0.282530	0.000025	0.000410	0.000011	0.009507	0.000328	440	1.01	1.36	0.28253	0.99
6	0.282512	0.000026	0.000630	0.000008	0.015575	0.000181	440	1.04	1.40	0.28251	0.27
7	0.282431	0.000026	0.001163	0.000026	0.029517	0.000841	440	1.17	1.58	0.28242	−2.41
8	0.282505	0.000028	0.000997	0.000016	0.024249	0.000337	440	1.06	1.42	0.2825	−0.04
9	0.282482	0.000027	0.001176	0.000015	0.030271	0.000409	440	1.09	1.48	0.28247	−0.95
10	0.282375	0.000030	0.001479	0.000045	0.036017	0.001270	440	1.26	1.72	0.28236	−4.71
11	0.282420	0.000029	0.001606	0.000097	0.042798	0.002597	440	1.20	1.62	0.28241	−3.23
12	0.282509	0.000026	0.000547	0.000003	0.012441	0.000072	440	1.04	1.40	0.2825	0.32
13	0.282475	0.000029	0.001172	0.000014	0.027791	0.000364	440	1.10	1.49	0.28247	−1.20
MME											
1	0.282393	0.000028	0.002096	0.000025	0.050948	0.000620	440	1.25	1.69	0.28238	−4.35
2	0.282518	0.000032	0.000701	0.000005	0.015667	0.000114	440	1.03	1.39	0.28251	0.51
3	0.282460	0.000027	0.001076	0.000007	0.025621	0.000180	440	1.12	1.52	0.28245	−1.65
4	0.282535	0.000025	0.000747	0.000011	0.016356	0.000217	440	1.01	1.35	0.28253	1.09
5	0.282509	0.000045	0.000760	0.000011	0.017502	0.000274	440	1.04	1.41	0.2825	0.18
6	0.282436	0.000028	0.000987	0.000006	0.021890	0.000162	440	1.15	1.60	0.28243	−2.45
7	0.282470	0.000029	0.000477	0.000003	0.010655	0.000088	440	1.09	1.50	0.28247	−1.01
8	0.282564	0.000046	0.001308	0.000029	0.029339	0.000674	440	0.98	1.30	0.28255	1.99
9	0.282483	0.000031	0.000718	0.000013	0.015788	0.000273	440	1.08	1.47	0.28248	−0.78
10	0.282515	0.000035	0.001126	0.000027	0.025492	0.000592	440	1.05	1.40	0.28251	0.37
Granodiorite porphyry											
1	0.282542	0.000029	0.002467	0.000015	0.056654	0.000408	440	1.05	1.37	0.28252	0.83
2	0.282542	0.000024	0.000860	0.000014	0.018445	0.000356	440	1.00	1.34	0.28254	1.31
3	0.282402	0.000028	0.000821	0.000013	0.017545	0.000296	440	1.20	1.65	0.28239	−3.66
4	0.282469	0.000025	0.001120	0.000015	0.026169	0.000363	440	1.11	1.50	0.28246	−1.35
5	0.282460	0.000025	0.000944	0.000002	0.021343	0.000060	440	1.12	1.52	0.28245	−1.63
6	0.282525	0.000030	0.002360	0.000123	0.056657	0.003141	440	1.07	1.40	0.28251	0.26
7	0.282473	0.000027	0.000594	0.000007	0.014502	0.000205	440	1.09	1.49	0.28247	−1.06
8	0.282538	0.000028	0.001339	0.000027	0.029043	0.000677	440	1.02	1.36	0.28253	1.01
9	0.282487	0.000024	0.001482	0.000077	0.034594	0.001836	440	1.10	1.47	0.28247	−0.82
10	0.282285	0.000039	0.000789	0.000027	0.018009	0.000543	440	1.36	1.91	0.28228	−7.77
11	0.282495	0.000025	0.001560	0.000067	0.036304	0.001741	440	1.09	1.45	0.28248	−0.56

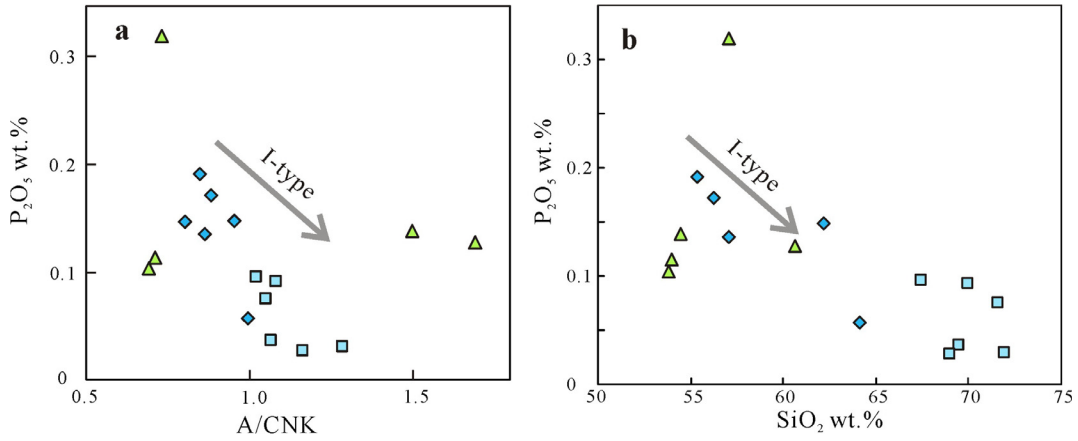

Fig. 6. Plots of (a) A/CNK vs. P_2O_5 and (b) SiO_2 vs. P_2O_5 for the granodioritic rocks and MMEs from the Shedongore district.

formation of the tectonic stress field and detailed geological processes after the collision of the Yangtze and Cathaysian blocks remain poorly constrained (Shu et al., 2008; Faure et al., 2009; Zhang et al., 2009; Charvet et al., 2010).

Early Paleozoic granitoids are widespread in the Guangxi region of southern China. Due to the absence of contemporaneous primitive magmas, the tectonic setting of the granitoids remains controversial (Bureau of Geology and Mineral Resources of Guangxi Zhuang Autonomous Region, 1985; Zhou, 2003; Li et al., 2006; Sun, 2006; Chen et al., 2011). In the Dayaoshan Uplift area the granitoid plutons previously mapped as small-scale apophyses and veins are actually large in size. In fact, these plutons extend as an igneous group over an area of 1500 km^2 (Chen et al., 2015). Geophysical studies have also revealed that a large batholith is hidden at depth in the study area (Zeng, 1996), suggesting that the small exposures of plutons on the surface may just be a shallow extension (stocks or veins) of large, deep-seated batholiths. Studies of magmatic rocks in the Wuyi–Yunkai Block and northern Guangdong Province have suggested that the tectonic transition from collision and extrusion to post-orogenic extension occurred at ca.

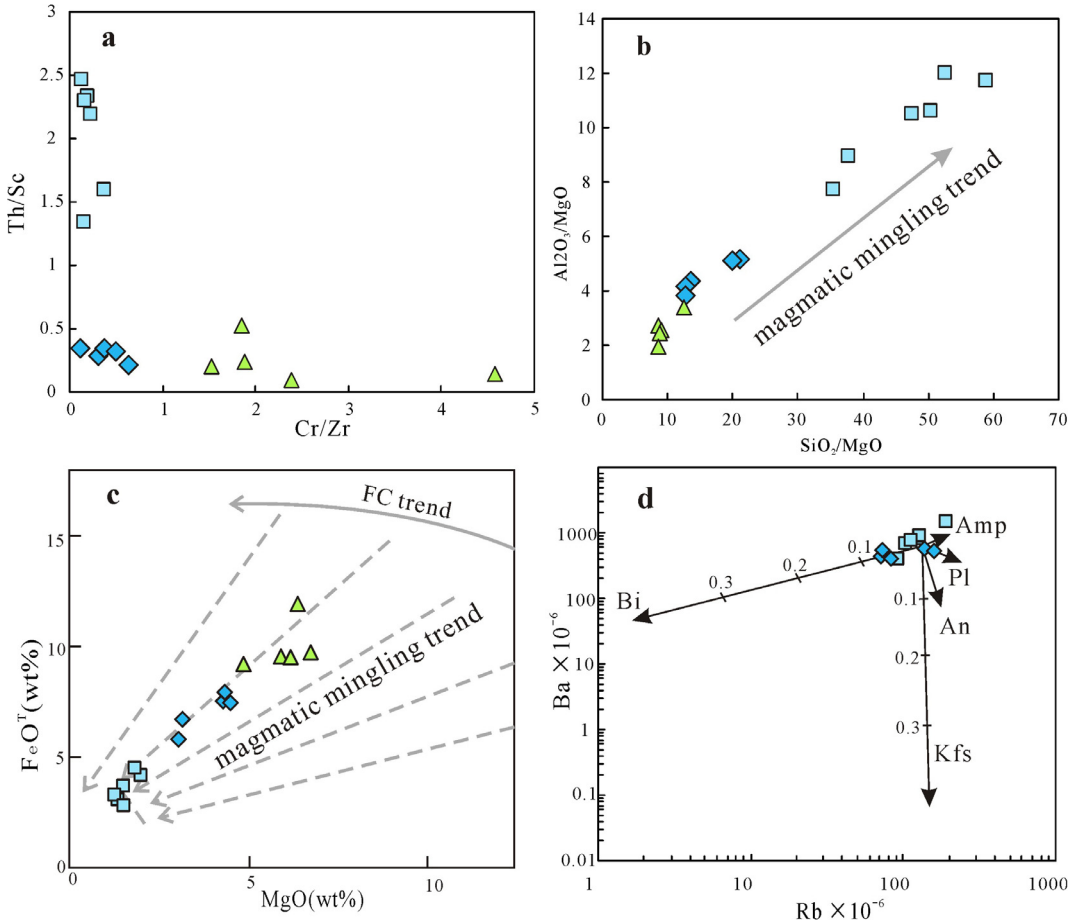

Fig. 7. Geochemical classification diagrams for the granodioritic rocks and MMEs from the Shedong ore district. (a) Cr/Zr vs. Th/Sc; (b) SiO_2/MgO vs. Al_2O_3/MgO; (c) MgO vs. FeO^T after Zorpi (1989); (d) Rb vs. Ba after Hanson and Sun (1976) and Ewart (1994).

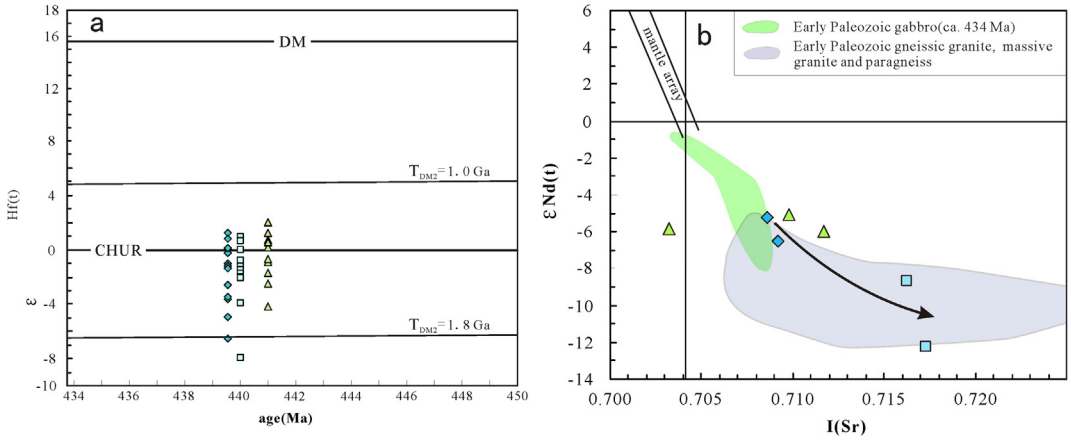

Fig. 8. (a) Age vs. $\varepsilon_{Hf}(t)$ diagram after Nowell et al. (1998) and Vervoort and Blichert-Toft, 1999. (b) I(Sr) vs. $\varepsilon_{Nd}(t)$ diagram. Data for gabbro, gneissic granite, massive granite, and paragneiss are from Wang et al.(2011, 2013), Wu et al.(2008), Zhang et al.(2012), and Huang et al.(2013b).

430–425 Ma (Shu et al., 2008; Zhang et al., 2009; Wang et al., 2011), and that lithospheric delamination and asthenosphere underplating were driven by post-orogenic collapse (Yao et al., 2012; Wang et al., 2013). In addition, the existence of Early Paleozoic high-Mg basalts in northern Guangdong Province (ca. 435 Ma) (Yao et al., 2012) and the lamprophyre found near the Daning pluton in northeastern Guangxi (ca. 440 Ma) (Wang, 2014) indicate an extensional regional tectonic setting during the Early Paleozoic.

The Shedong granodioritic rocks and their MMEs have similar ages (ca. 440 Ma). Geochemical characteristics of the granodioritic rocks are similar to those in Daning, Gulong, Gupao, and Taohua of northeastern Guangxi, as reported by Wang (2014), Li et al. (2006), Liu (1993) and Zeng et al. (1993), indicating a crust–mantle mixing origin. These previous studies also confirmed that mingling of magmas derived from the crust and mantle played an important role in the formation of Early Paleozoic granitoids in

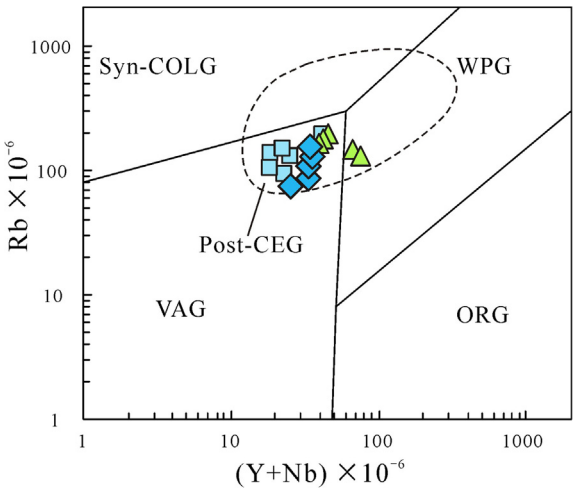

Fig. 9. (Y + Nb) vs. Rb discrimination diagram after Pearce et al. (1984) and Forster et al. (1997) for granodioritic rocks and MMEs of the Shedong ore district.

southern China (Lou et al., 2002; Xu et al., 2007; Cheng et al., 2012). These large-scale I-type granitoids (e.g., diorite) with these petrogenetic features are consistent with an origin in an extensional setting.

On tectonic discrimination diagrams (Fig. 9), data for samples of the Shedong ore district plot within the post-collisional extensional field. Based on this result, combined with the above discussion, we propose that the calc-alkaline I-type granitoids in the Shedong ore district were produced by the re-melting of middle Proterozoic crust as a result of underplating of mantle-derived magma, and magma mingling occurred during the tectonic transition from collision and extrusion to post-orogenic extension in the Early Paleozoic. The mantle-derived magmas played an important role in the formation of the early Paleozoic granodioritic rocks and MMEs via their heat and material input.

7. Conclusions

A geochronological, geochemical, and isotopic study of the ore-forming granodioritic plutons and their MMEs from the Baoshan and Pingtoubei ore deposits has led to the following main conclusions.

(1) We obtained new zircon U–Pb ages of 439.8 ± 3.2 and 441.1 ± 2.2 Ma for a granodiorite and its MME from the Baoshan deposit, and 440.0 ± 1.7 Ma for a granodiorite porphyry from the Pingtoubei deposit in the Shedong ore district of Guangxi, southern China. These ages are all within error of each other and are indicative of pluton emplacement during the early Silurian (ca. 440 Ma).

(2) The granodiorites and its MMEs from the Baoshan deposit are calc-alkaline I-type granitoids. Their parental magmas were probably generated through re-melting of middle Proterozoic crust as a result of underplating of mantle-derived magmas during the tectonic transition from a collisional to post-orogenic extensional setting. Varying degrees of magma mingling between crust-and mantle-derived melts contributed to the formation of the granodioritic rocks and MMEs.

Acknowledgements

This study was supported by the DREAM project of MOST of China (Grant No. 2016YFC0600407), the National Natural Science Foundation of China (Grant Nos. 41463001 and 41572191), the Natural Science Foundation of Guangxi (Grant Nos. 2016GXNSFAA380012, 2015GXNSFDA139029, 2015GXNSFBA139205 and 2012GXNSFBA053132), the Program of Collaborative Innovation Center for Exploration of Hidden Nonferrous Metal Deposits and Development of New Materials in Guangxi and a Bagui Scholarship Innovation Project of Guangxi (Xu Jifeng, 2013).

References

Beloisova, B.A., Griffin, W.L., O'Reilly, S.Y., 2006. Zircon crystal morphology, trace element signatures and Hf isotope composition as a tool for petrogenetic modeling: examples from Eastern Australian granitoids. J. Petrol. 47 (2), 329–353.

Bureau of Geology and Mineral Resources of Guangxi Zhuang Autonomous Region, 1985. Regional geology of Guangxi Zhuang autonomous region, People's Republic of China. Geological Publishing House, Beijing, 1–96 (in Chinese with English abstract).

Bolhar, R., Weaver, S.D., Whitehouse, M.J., Palin, J.M., Woodhead, J.D., Cole, J.W., 2008. Sources and evolution of arc magmas inferred from coupled O and Hf isotope systematics of plutonic zircons from the Cretaceous Separation Point Suite (New Zealand). Earth Planet. Sci. Lett. 268 (3–4), 312–324.

Castro, A., Moreno-ventas, I., 1991. H-type (hybrid) Granitoids: a proposed revision of the granite-type classification and nomenclature. Earth Sci. Rev. 31 (3), 237–253.

Charvet, J., Shu, L.S., Faure, M., Choulet, F., Wang, B., Lu, H.F., Breton, N.L., 2010. Structural development of the lower paleozoic belt of south China: genesis of an intracontinental orogen. JAES 39, 309–330.

Chappell, B.W., White, A.J.R., 1974. Two contrasting granite type. Pacific Geol. 8, 173–174.

Chappell, B.W., White, A.J.R., 1992. I-and S-type granites in the lachlan fold belt. Trans. Royal Soc. Edinburgh: Earth Sci. 83, 1–26.

Chen, M.H., Mo, C.S., Huang, Z.Z., Li, B., Huang, H.W., 2011. Zircon LA-ICP-MS U-Pb ages of granitoid rocks and molybdenite Re-Os age of Shedong W-Mo deposit in Cangwu County of Guangxi and its geological significance. Mineral Deposits 30 (6), 963–978 (in Chinese with English abstract).

Chen, M.H., Huang, Z.Z., 2012. Geochemistry of granitoid rocks of Shedong W-Mo deposit district in Cangwu County, Guangxi and its relation to mineralization. Acta Petrol. Sin. 28 (1), 199–212 (in Chinese with English abstract).

Chen, M.H., Li, Z.Y., Li, Q., 2015. A preliminary study of multi-stage granitoids and related metallogenic series in Dayaoshan area of Guangxi, China. Earth Sci. Front. 22 (2), 41–53 (in Chinese with English abstract).

Cheng, S.B., Fu, J.M., Cheng, X.Q., Ma, L.Y., 2012. Zircon SHRIMP U-Pb dating and geochemical characteristics of Haiyangshan Monzogranitic Batholith, Northeast Guangxi. Geol. Miner. Resour. South China 2, 132–140 (in Chinese with English abstract).

Cui, B., Zhai, Y.S., Meng, Y.F., 2000. Transformation of mesozoic tectonic domain and its relation to mineralization in Southeastern China: an evidence of Southeastern Fujian Province. Earth Sci. – J. China Univ. Geosci. 25 (4), 352–355 (in Chinese with English abstract).

Deng, J., 2012. Mineralization regularity of the copper-gold polymetallic deposits in Dayaoshan, Guangxi. China Geol. Resour. 21 (3), 302–307 (in Chinese with English abstract).

Ewart, G.W.L., 1994. A application of proton-microprobe data to Trace-element partitioning in Volcanic Rocks. Chem. Geol. 117, 251–284.

Faure, M., Shu, L.S., Wang, B., Charvet, J., Choulet, F., Monie, P., 2009. Intracontinental subduction: a possible mechanism for the Early Palaeozoic Orogen of SE China. Terra Nova 21 (5), 360–368.

Forster, H.J., Tischendorf, G., Trumbull, R.B., 1997. An evaluation of the Rb vs. (Y + Nb) discrimination diagram to infer tectonic setting of silicic igneous rocks. Lithos 40, 261–293.

Griffin, W.L., Wang, X., Jackson, S.E., Person, N.J., O'Reilly, S.Y., Xu, X., 2002. Zircon chemistry and magma mixing, SE China: in-situ analysis of Hf isotopes, Tonglu and Pingtan igneous complexes. Lithos 61 (3), 237–269.

Griffin, W.L., Pearson, N.J., Belousova, E.A., Saeed, A., 2007. Reply to "Comment to short-communication 'Comment: Hf-isotope heterogeneity in zircon 91500' by W.L. Griffin, N.J. Pearson, E.A. Belousova and A. Saeed (Chemical geology 233 (2006) 358-363)" by F. Corfu. Chem. Geol. 244 (1–2), 350–353.

Guo, L.Z., Shi, Y.S., Ma, R.S., 1984. Tectonostratigraphic Terranes of Southeast China. J. Nanjing Univ. (Nat. Sci. Edit.) 20 (4), 732–739 (in Chinese with English abstract).

Hanson, G.N., Sun, S.S., 1976. Race earth element evidence for differentiation of McMundo volcanics, Ross Island, Antarctica. Contrib Mineral Petrol. 54, 139–155.

He, Z.Y., Xu, X.S., Niu, Y.L., 2010. Petrogenesis and tectonic significance of a Mesozoic granite-syenite-gabbro association from inland South China. Lithos 119 (3–4), 621–641.

Hu, Z.C., Gao, S., Liu, Y.S., Hu, S.H., Chen, H.H., Yuan, H.L., 2008. Signal enhancement in laser ablation ICP-MS by addition of nitrogen in the central channel gas. J. Anal. At. Spectrom. 23, 1093–1101.

Huang, X.L., Niu, Y.L., Xu, Y.G., Ma, J.L., Qiu, H.N., 2013a. Geochronology and geochemistry of cenozoic basalts from Eastern Guangdong, Se China: constraints on the lithosphere evolution beneath the northern margin of the South China Sea. Contrib. Miner. Petrol. 165 (3), 437–455.

Huang, X.L., Yu, Y., Li, J., Tong, L.X., Chen, L.L., 2013b. Geochronology and petrogenesis of the early paleozoic I-type granite in the taishan area, south china: middle-lower crustal melting during orogenic collapse. Lithos 177 (3), 268–284.
Jiang, X.Z., Kang, Z.Q., Xu, J.F., Xiong, S.Q., Wu, J.C., 2015. LA-(MC)-ICP-MS zircon U-Pb dating of porphyry from Baoshan copper deposit of Dayaoshan uplift area in Guangxi. J. Guilin Univ. Technol. 35 (4), 766–773 (in Chinese with English abstract).
Kemp, A.I., Whitehouse, M.J., Hawkesworth, C.J., Alarcon, M.K., 2005. A zircon U-Pb study of metaluminous (I-type) granites of the Lachlan Fold Belt, southeastern Australia: implications for the high/low temperature classification and magma differentiation processes. Contrib. Miner. Petrol. 150 (2), 230–249.
Kemp, A.I., Hawkesworth, C.J., Foster, G.L., Paterson, B.A., Woodhead, J.D., Hergt, J.M., Gray, C.M., Whitehouse, M.J., 2007. Magmatic and crustal differentiation history of granitic rocks from Hf-O isotopes in zircon. Science 315 (5814), 980–983.
Koyaguchi, T., Blake, S., 1991. Origin of Mafic Enclaves: Constraints on the Magma Mixing Model from F1 Dynamic Experiments. Enclaves in Granite Petrology. Elsevier, Amsterdam, pp. 415–429.
Li, W., Bi, S.J., Yang, Z., et al., 2015. Zircon U-Pb age and Hf Isotope characterization of Sheshan Granodiorite in Southern Edge of Dayaoshan, Guidong: constraints on caledonian diagenesis and mineralization. Earth Sci. Front. 40 (1), 17–33 (in Chinese with English abstract).
Li, W.J., Liang, J.C., Feng, Z.H., 2006. Judging for characteristics of geochemical and structural environment of several Caledonian granitoids in northeast Guangxi. Mineral Resour. Geol. 20 (4–5), 353–360 (in Chinese with English abstract).
Li, X.H., Liu, Y., Tu, X.L., 2002. Precise determination of chemical compositions in silicate rocks using ICP AES and ICP MS: a comparative study of sample digestion techniques of alkali fusion and acid dissolution. Geochimica 31, 289–294 (in Chinese with English abstract).
Li, X.H., Liu, D.Y., Sun, M., Li, W.X., Liang, X.R., Liu, Y., 2004. Precise Sm-Nd and U-Pb isotopic dating of the supergiant Shizhuyuan polymetallic deposit and its host granite, SE China. Geol. Mag. 141, 225–231.
Li, X.H., Qi, C.S., Liu, Y., Liang, X., Tu, X.L., 2005. Petrogenesis of the Neoproterozoic bimodal volcanic rocks along the western margin of the Yangtze Block: new constraints from Hf isotopes and Fe/Mn ratios. Chi. Sci. Bull. 50, 2481–2486.
Liu, G.Q., Cai, M.H., 2004. Ore-forming condition and genetic analysis on the gold deposit in Dayaoshan Region, Eastern Guangxi. Geol. Sci. Technol. Inform. 23 (2), 37–44 (in Chinese with English abstract).
Liu, T.F., 1993. The characteristics of granitoid in east Guangxi and its relation with gold deposit. Guangxi Geol. 6 (4), 77–86 (in Chinese with English abstract).
Liu, Y., Liu, H.C., Li, X.H., 1996. Simultaneous and Precise Determination of 40 Trace Elements in Rock Samples Using ICP-MS. Geochimica 25, 552–558 (in Chinese with English abstract).
Liu, Y.S., Hu, Z.C., Gao, S., Gunther, D., Xu, J., Gao, C.G., Chen, H.H., 2008. In situ analysis of major and trace elements of anhydrous minerals by LA-ICP-MS without applying an internal standard. Chem. Geol. 257, 34–43.
Liu, Y.S., Gao, S., Hu, Z.C., Gao, C.G., Zong, K.Q., Wang, D., 2010. Continental and oceanic crust recycling-induced melt peridotite interactions in the Trans-North China Orogen: U-Pb dating, Hf isotopes and trace elements in zircons of mantle xenoliths. J. Petrol. 51, 537–571.
Lou, F.S., Shu, L.S., Wang, D.Z., 2002. The Mesozoic Wugongshan granitic dome extensional tectonics and petro-geochemistry. Geol. Bull. China 21, 264–269 (in Chinese with English abstract).
Lou, L., Jiang, S.Y., Yang, S.Y., Zhao, K.D., Wang, S.L., 2010. Petrochemistry, zircon U-Pb dating and Hf isotopic composition of the granitic pluton in the Pengshan Sn-polymetallic orefield, Jiangxi Province. Acta Petrol. Sin. 26 (9), 2818–2834 (in Chinese with English abstract).
Ludwig, K.R., 2003. Isoplot: a geochronological toolkit for Microsoft Excel. Berkeley Geochronology Center Special Publication, No. 4, pp. 1–67.
Maniar, P.D., Piccoli, P.M., 1989. Tectonic discrimination of granitoids. Geol. Soc. Am. Bull. 101 (5), 635–643.
McArthur, J.M., 1994. Recent trends in strontium isotope stratigraphy. Terra Nova 6, 331–358.
McDonough, W.F., Sun, S.S., 1995. The composition of the earth. Chem. Geol. 120 (3), 223–253.
Middlemost, E.A.K., 1985. Magmas and Magmatic Rocks. Longman, London. l-266.
Nitoi, E., Munteanu, M., Marice, S., Paraschivoiu, 2002. Magma enclave interactions in the East Carpathian Subvolcanic Zone, Romania: petrogenetic implications. J. Volcanol. Geotherm. Res. 118 (1–2), 229–259.
Nowell, G.M., Kempton, P.D., Noble, S.R., Fitton, J.G., Saunders, A.D., Mahoney, J.J., 1998. High precision Hf isotope measurements of MORB and OIB by thermal ionisation mass spectrometry: insights into the depleted mantle. Chem. Geol. 149 (3–4), 211–233.
Pearce, J., Harris, N.B.W., Tindle, A.G., 1984. Trace element discrimination diagrams for the tectonic interpretation of granitic rocks. J. Petrol. 25, 956–983.
Peccerillo, A., Taylor, S.R., 1976. Geochemistry of Eocene calc-alkaline volcanic rocks from the Kastamonu area, Northern Turkey. Contrib. Miner. Petrol. 58, 63–81.
Peng, S.B., Jin, Z.M., Liu, Y.H., Fu, J.M., He, L.Q., 2006. Petrochemistry, chronology and tectonic setting of strong Peraluminous Anatectic Granitoids in Yunkai Orogenic Belt, Western Guangdong Province, China. Earth Sci. – J. China Univ. Geosci. 31 (1), 110–120 (in Chinese with English abstract).
Perugini, D., Poli, G., Christofids, G., Eleftheriadis, G., 2003. Magma mixing in the Sithonia Plutonic Complex, Greece: evidence from mafic microgranular enclaves. Mineral. Petrol. 78 (3–4), 173–200.
Ren, J.S., 1990. On the geotectonic of Southern China. Acta Geol. Sin. 4, 275–288 (in Chinese with English abstract).
Ren, J.S., Jiang, C.F., Zhang, Z.K., 1980. Geotectonic Evolution of China. Science Press. 1-140 (in Chinese with English abstract).
Shu, L.S., Yu, J.H., Jia, D., Wang, B., Shen, W.Z., 2008. Early Paleozoic orogenic belt in the eastern segment of South China. Geol. Bull. China 27 (10), 1581–1593 (in Chinese with English abstract).
Sun, T., 2006. A new map showing the distribution of granites in South China and its explanatory notes. Geol. Bull. China 25 (3), 332–335 (in Chinese with English abstract).
Sunagawa, K.A., 1985. A model for mixing basaltic and dacitic magmas as deduced from experimental data. Contrib. Miner. Petrol. 89 (l), 17–23.
Tannaka, T., Togashi, S., Kamioka, H., Amakawa, H., Kagami, H., 2000. JNdi-1: a neodymium isotopic reference in consistency with LaJolla neodymium. Chem. Geol. 168, 279–281.
Vernon, R.H., 1983. Restite, Xenoliths and Microgranitoid Enclaves in Granites.
Vervoort, J.D., Blichert-Toft, J., 1999. Evolution of the depleted mantle: Hf isotope evidence from juvenile rocks through time. Geochim. Cosmochim. Acta 63 (3–4), 533–556.
Wang, L., 2014. Chronology, petrology, geochemistry and petrogenesis of Daning granitic pluton and its mafic enclaves, northeast Guangxi. China Academy of Geological Sciences Master Thesis.
Wang, Y.J., Fan, W.M., Sun, M., Liang, X., Zhang, Y., 2007. Geochronological, geochemical and geothermal constraints on petrogenesis of the Indosinian peraluminous granites in the South China Block: a case study in the Hunan Province. Lithos 96 (3–4), 475–502.
Wang, Y.J., Zhang, A., Fan, W.M., Zhao, G., Zhang, G., 2011. Kwangsian Crustal Anatexis within the Eastern South China Block: geochemical, zircon geochronological and Hf Isotopic fingerprints from the gneissoid granites of Wugongand Wuyi-yunkai Domains. Lithos 127 (1), 239–260.
Wang, Y.J., Zhang, A., Fan, W.M., 2013. Origin of Paleosubduction-modified mantle for Silurian gabbro in the cathaysia block: geochronological and geochemical evidence. Lithos 160, 37–54.
Watson, E.B., Harrison, T.M., 1983. Zircon saturation revisited: temperature and composition effects in a variety of crustal magma types. Earth Planet. Sci. Lett. 64, 295–304.
Wei, G.J., Liang, X.R., Li, X.H., Liu, Y., 2002. Precise measurement of Sr isotopic composition of liquid and solid base using (LP) MC-ICPMS. Geochimica 31, 295–299 (in Chinese with English abstract).
Wei, Z.R., Huang, Y.P., Ye, Y.L., 2012. Mineralization feature and prospecting direction of Dali molybdenum deposit, Tenxian, Guangxi Province. Geol. Miner. Resour. South China 28 (4), 383–391 (in Chinese with English abstract).
Wiedenbeck, M., Alle, P., Corfu, F., Griffin, W.L., Meier, M., Oberli, F., Quadt, A.V., Roddick, J.C., Spiegel, W., 1995. Three natural zircon standards for U-Th-Pb, Lu-Hf, trace element and REE analyses. Geostand. Geoanal. Res. 19, 1–23.
Wilson, M., 1989. Igneous Petrogenesis. Allen and Unwin, London.
Woodhead, J.D., Hergt, J.M., 2005. A preliminary appraisal of seven natural zircon reference materials for in situ Hf isotope determination. Geostand. Geoanal. Res. 29 (2), 183–195.
Wu, F.Y., Li, X.H., Zheng, Y.F., Gao, S., 2007a. Lu-Hf isotopic systematics and their applications in petrology. Acta Petrol. Sin. 23 (2), 185–220 (in Chinese with English abstract).
Wu, F.Y., Li, X.H., Yang, J.H., Zheng, Y.F., 2007b. Discussions on the petrogenesis of granites. Acta Petrol. Sin. 23 (6), 1217–1238 (in Chinese with English abstract).
Wu, G.Y., Ma, T.Q., Feng, Y.F., Yan, Q.E., Liu, F.G., Bo, D.Y., 2008. Geological and geochemical characteristics and genesis of the Caledonian Wanyangshan granite in the Nanling Mountains, South China. Geol. China 35 (4), 608–617.
Wyllie, P.J., Cox, K.G., Biggar, G.M., 1962. The habit of apatite in synthetic systems and igneous rocks. J. Petrol. 3 (2), 238–242.
Xie, Y.C., Lu, J.J., Ma, D.S., 2013. Origin of granodiorite porphyry and mafic microgranular enclave in the Baoshan Pb-Zn polymetallic deposit, southern Hunan Province: Zircon U-Pb chronological, geochemical and Sr-Nd-Hf isotopic constraints. Acta Petrol. Sin. 29 (12), 4186–4214 (in Chinese with English abstract).
Xu, D.R., Xia, B., Li, P.C., Chen, G.H., Ma, C., Zhang, Y.Q., 2007. Protolith natures and U-Pb sensitive high mass-resolution ion microprobe (SHRIMP) zircon ages of the metabasites in Hainan Island, South China: implications for geodynamic evolution since the late precambrian. Island Arc. 16 (4), 575–597.
Yang, J.H., Wu, F.Y., Wilde, S.A., Xie, L.W., Yang, Y.H., Liu, X.M., 2007. Tracing magma mixing in granite genesis: in situ U-Pb dating and Hf-isotope analysis of zircons. Contrib. Miner. Petrol. 153 (2), 177–190.
Yang, M.G., Mei, Y.W., 1997. Characteristics of geology and metallization in the Qinzhou-Hangzhou Paleoplate Juncture. Geol. Miner. Resour. South China 3, 52–59 (in Chinese with English abstract).
Yang, M.G., Huang, S.B., LOU, F.S., Tang, W.X., Mao, S.B., 2009. Lithospheric structure and large-scale metallogenic process in Southeast China continental area. Geol. China 36 (3), 528–543 (in Chinese with English abstract).
Yao, W.H., Li, Z.X., Li, W.X., Wang, X.C., Li, X.H., Yang, J.S., 2012. Post-kinematic Lithospheric Delamination of the Wuyi-yunkai Orogen in South China: Evidence from Ca. 435 ma High-Mg Basalts. Lithos 154, 115–129.
Zeng, C.Y., Xiao, L., Ye, N.Q., Hu, C.Y., Liu, C., Cai, L.X., 1993. The geological and minerogenic characteristics of the granitoids in the Lingjiao area, Cangwu, Guangxi. J. Guilin College Geol. 13 (4), 340–349 (in Chinese with English abstract).
Zeng, C.Y., 1996. The relation of the feature of the deep structure to gold mineralization in the upwarping region of Dayao Mountain in eastern Guangxi. J. Guilin Inst. Technol. 16 (3). 245-25 (in Chinese with English abstract).

Zhang, F.R., Shu, L.S., Wang, D.Z., Yu, J.H., Shen, W.Z., 2009. Discussions on tectonic setting of Caledonian granitoids in the eastern segment of South China. Earth Sci. Front. 1, 248–260 (in Chinese with English abstract).

Zhang, F.F., Wang, Y.J., Zhang, A.M., Fan, W.M., Zhang, Y.Z., Zi, J.W., 2012. Geochronological and geochemical constraints on the petrogenesis of Middle Paleozoic(Kwangsian) massive granites in the eastern South China Block. Lithos 150 (1), 188–208.

Zhang, Z.Q., Chen, M.H., MO, J.M., Xiao, L.Y., Huang, Z.Z., 2014. Evolution and source tracing of the Shedong quartz vein type scheelite molybdenite polymetallic deposit in Cangwu County, Guangxi. Acta Petrol. Sin. 30 (1), 281–291 (in Chinese with English abstract).

Zhong, L.F., Xia, B., Liu, L.W., Li, J., Lin, X.G., 2010. Metallogenic geochronology of Yuanzhuding Cu–Mo deposit in western Guangdong eastern Guangxi metallogenic belt and its geological significance. Mineral Deposits 29 (3), 395–404 (in Chinese with English abstract).

Zhou, X.M., 2003. My thinking about granite geneses of South China. Geol. J. China Univ. 9 (4), 556–565 (in Chinese with English abstract).

Zhu, J.C., Zhang, P.H., Xie, C.F., 2006. Magma mixing origin of the mafic enclaves in Lisong Granite, NE Guangxi, western Nanling Mountains. Geochimica 35 (5), 506–516 (in Chinese with English abstract).

Zhu, J.C., Wang, R.C., Zhang, P.H., Xie, C.F., Zhang, W.L., Zhao, K.D., Xie, L., Yang, C., Che, X.D., Wang, L.B., 2009. Zircon U-Pb geochronological framework of Qitianling granite batholith, middle part of Nanling Range, South China. Sci. China (Series D) 52 (9), 1279–1294.

Zorpi, M.J., 1989. Magma mingling, zoning and emplacement in calc-alkaline granitoid pluton. Tectonophysics 157, 315.